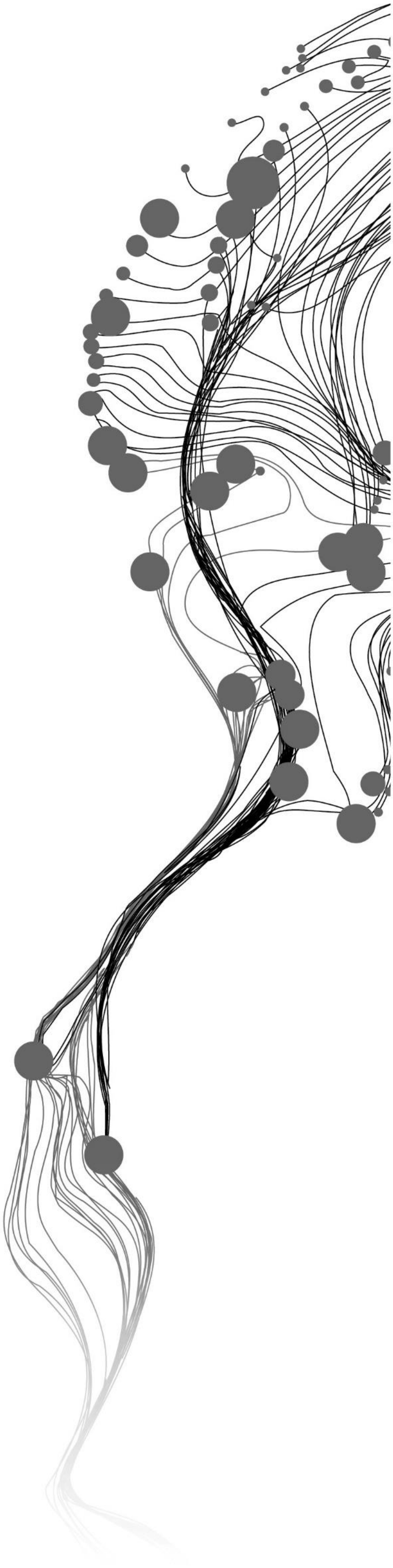

Developing a worst-case Tropical Cyclone rainfall scenario for flood on Dominica

HELEN NGONIDZASHE SERERE
Enschede, The Netherlands, August 2020

Thesis submitted to the Faculty of Geo-Information Science and Earth Observation of the University of Twente in partial fulfilment of the requirements for the degree of Master of Science in Spatial Engineering.

SUPERVISORS:
Dr. Ir. Janneke Ettema
Prof. Dr. Victor Jetten

THESIS ASSESSMENT BOARD:
Prof. Dr. Norman Kerle (Chair)
Dr. Rein Haarsma (External Examiner, KNMI)

ABSTRACT

Fresh water flooding as a result of tropical cyclone rainfall depicts a hydrometeorological hazard that needs to be prepared against. When not adequately prepared for, freshwater flooding results in immense damages that disrupts economies, displace settlements, and increase the poverty line. To prepare and mitigate against tropical cyclone (TC) induced freshwater flooding, countries make use of design storms. One disadvantage, however, is that design storms are very different from actual storm events with respect to both spatial and temporal rainfall structures. Design storms tend to lose vital storm information which influences the results of the simulated flood hazards. When dealing with extreme rainfall events, the simplification of storm traits by design storm may result in major implications on the decisions made for flood mitigations owing to the differences in simulated flood characteristics between the design storm and the extreme rainfall event.

This research intended to evaluate the flood implications of simulating a worst-case tropical cyclone rainfall scenario against a design storm of comparable rainfall characteristics. Using the Southern catchments of Dominica as a study area and the 2017 Atlantic basin TC Maria as a proof of concept, the research was carried out in two main steps. First a method was developed to extract extreme rainfall pixels from the passage of a TC given temporal layers of precipitation images. Using the extracted extreme rainfall pixels and Dominica's 100-year design storm, flood characteristics of the TC scenarios and the design storm were compared. Based on the flood characteristics of the worst-case rainfall scenario (extreme TC rainfall pixel with the highest simulated flood characteristics) and the 100-year design storm, economic flood implications of simulating a flood from the two approaches are evaluated.

Contrary to common perception, the results of the analysis showed the extreme rainfall pixels of TC Maria to result from a category 2 and 3 cyclones. Of the extreme TC rainfall pixels used as TC scenarios, the worst-case rainfall scenario resulted from a high intensity pixel with a maximum intensity of 107mm/hr, three peak intensity values, and a shortest distance from the TC eye of 10km. Comparisons made between the flood characteristics of the TC scenarios and the 100-year design storm showed the 100-year design storm to have overall shorter flood start times, higher flood volume, larger flooded areas and higher flood heights in comparison to the TC scenarios. Based on the obtained flood characteristics, the 100-year design storm was concluded to simulate overestimated flood characteristics which would imply overestimated flood mitigation measures.

KEYWORDS

Tropical Cyclone rainfall, Extreme Rainfall Pixels, Flood Characteristics, Global Precipitation Mission (GPM), Open LISEM.

ACKNOWLEDGEMENTS

At the very beginning, I would like to thank the Almighty God for giving me the strength and the composure to complete this thesis within the scheduled time. I would also like to express my deepest gratitude to my mother (Julien Harusekwi Serere) for her sacrifices and constant support throughout all my studies.

During the course of my studies, I have received enormous help from many quarters, which I would like to put on record here with sincere gratitude and great pleasure. First and foremost, I am grateful to my supervisors, Dr Ir. Janneke Ettema and Prof. Dr Victor Jetten. These two allowed me to encroach upon their precious time freely, from the very beginning till the completion of my thesis. Their guidance, encouragement and suggestions provided me with necessary insights and paved the way for the meaningful ending of this master's degree.

I also give much credit to the ITC-UT, which provided me with the excellence scholarship, enabling my study dream to become a reality. Additionally, I would like to thank the Spatial Engineering staff, which I will, however, fail to mention by name due to their numbers, for their academic mentoring. I have no hesitation in saying that, without their constant support and valuable advice from time-to-time, I would have failed to complete and achieve all that I did during this period.

Last but not least, my thanks and appreciations go to my colleagues and everyone who gave their suggestions and offered their help different ways.

Helen Ngonidzashe Serere
Enschede, 2020

TABLE OF CONTENTS

LIST OF FIGURES

LIST OF TABLES

LIST OF ACRONYMS

CHARIM:	Caribbean Handbook on Risk Information Management
D.S	Design Storm
DEM:	Digital Elevation Model
GIS:	Geographic Information System
GPM:	Global Precipitation Mission
IBTrACS:	International Best Track Archive for Climate Stewardship
IDF:	Intensity Duration Frequency
IMERG:	Integrated Multi-satellite Retrievals for GPM
IPCC:	Intergovernmental Panel on Climate Change
LDD:	Local Drainage Network
LISEM:	Limburg Soil Erosion Model
MSW:	Maximum Sustained Wind
NASA:	National Aeronautics and Space Administration
NHC:	National Hurricane Centre
TC:	Tropical Cyclone
TRMM:	Tropical Rainfall Measuring Mission

DEFINITION OF TERMS

As a clarification to the terms used in this research, the following are hereby defined:

Tropical Cyclone: Any low-pressure system with a closed circulation originating over tropical oceans. The low-pressure systems are inclusive of tropical depressions, tropical storms, hurricanes, and extratropical cyclones.

Rainfall magnitude: Total tropical cyclone rainfall recorded within a pixel for the duration of the tropical cyclone rain bands over the pixel. For the design storm, the magnitude is defined as the total rainfall over the design storm's duration.

Maximum rainfall intensity: Highest intensity (rainfall produced per temporal resolution) recorded in a pixel for the duration of the tropical cyclone.

Extreme rainfall pixels: Pixels within the path of the tropical cyclone with the highest rainfall totals or the highest observed maximum rainfall intensities.

Worst-case rainfall scenario: An extreme rainfall pixel, from the passage of a TC, that produces the highest overall flood characteristics in comparison to other extreme rainfall pixels simulated.

CHAPTER 1 INTRODUCTION

Hazard awareness is one of the primary steps in creating resilient countries and communities (Tapsell et al., 2010; Teitelbaum, Ginsburg, & Hopkins, 2015). Knowing exactly when a hazard will occur, the magnitude of the hazard and high risk areas will no doubt go a long way in achieving resilience (Doswell III, 2015). With the world constantly changing, however, uncertainties in natural hazard forecasting can never be avoided. Hydrometeorological hazards for instance, are strongly influenced by changes in climatic conditions, land use changes, and the occurrence of large scale disasters which shift risk areas (Jayawardena, 2015). Despite, however, the lower likelihood of achieving precise detailed forecasts for natural hazards, countries need to keep striving to use the available uncertainties in making logical forecasts that are within practical means (Doswell III, 2015; Emanuel, 2017). One such hazard with high uncertainties that needs to be prepared against is freshwater flooding resulting from extreme precipitation events such as that brought about by tropical cyclones.

Freshwater flooding as a result of tropical cyclone (TC) rainfall, stands as one of the most destructive (Rappaport, 2014; Rappaport & Blanchard, 2016) and complicated natural disasters to prepare against (Doswell III, 2015; Emanuel, 2017). Unlike seasonal rainfall events which follow similar structural rainfall patterns (Tennant & Hewitson, 2002), TC rainfall is particularly erratic in occurrence (Emanuel, 2017; Jiang, Halverson, Simpson, & Zipser, 2008). The probability of occurrence of TC rainfall on a particular area is a combination of the probability of the TC appearing within the area, the trajectory of the TC, the distribution and extent of the TC rain bands, and the environmental factors which either amplify or de-amplify the rainfall potential (Balaguru, Foltz, & Leung, 2018; S. S. Chen, Knaff, & Marks, 2006; Ogden, 2016; Zhou & Matyas, 2018). Since frequency magnitude relations are derived from rainfall stations with an incidental location (Qi, Martinaitis, Zhang, & Cocks, 2016), the probability of TC rainfall being recorded is based on the probability of the rainfall station being in the trajectory of the TC rainfall and the recurrence of the TC with similar rainfall structure. The erratic nature and complexity of TC rainfall makes preparing and mitigating against TC induced flooding essentially difficult (Begueria, Vicente-Serrano, Lopez-Moreno, & Garcia-Ruiz, 2009; Emanuel, 2017).

Despite, however, the erratic nature and complexities of TC rainfall, countries still need to prepare against freshwater flooding. When not adequately prepared for, TC induced flooding results in large fatalities and immense damages that disrupts economies, displace settlements, and increase the poverty line (Blake, Landsea, Miami, & Gibney, 2011; Czajkowski, Villarini, Michel-Kerjan, & Smith, 2013; Prevatt, Dupigny-Giroux, & Masters, 2010). The social and economic distractions brought by TC induced flooding take communities years to recover from (Barclay et al., 2019; Collymore, 2011; Paul-Rolle, 2014). To minimize distractions, officials need to identify high risk areas beforehand for prioritization of rescue missions and for planning purposes (Jamrussri & Toda, 2018; Kim, Pant, & Yamashita, 2014; Opper, Cinque, & Daviesc, 2010). Knowing the magnitude of the expected flood hazard can help planners decide on the strength of the mitigation measures and decide on where to implement the required mitigation measures (Collymore, 2011; Doswell III, 2015; Lumbroso, Boyce, Bast, & Walmsley, 2011).

To prepare and mitigate against flooding, counties often make use of design storms (Balbastre-Soldevila, García-Bartual, & Andrés-Doménech, 2019; de Paola, Giugni, Topa, & Bucchignani, 2014; Lumbroso et al., 2011). Design storms are commonly made from Intensity-Duration-Frequency (IDF) curves. The IDF curves are constructed from ground based rainfall stations with rainfall records of preferably high temporal resolution, 5minute interval data, dating back to at least 20 years (Jetten, 2016; Lumbroso et al., 2011). Statistical analysis of the historical rainfall events computes for the rainfall return period of a particular storm. The return period is defined as the probability of occurrence and exceedance of a rainfall event of a given magnitude or intensity (rainfall in a given time) within a specified time frame (Ybañez, 2013). Based on the statistical characteristics of each return period, design storms associated with a particular return period are used to simulate flood hazard maps. The most highlighted advantages of using design storms are that they ensure uniform levels of quality and simplify hydrological and hydraulic calculations (Balbastre-Soldevila et al., 2019).

Design storms were originally used in civil engineering to determine peak discharge for rivers and for channel construction (Beguería & Vicente-Serrano, 2006; Lumbroso et al., 2011). In civil engineering applications, design storms are an accepted and well tested method. However, for flood hazard assessments, vast disadvantages exist. Through the uniformity of design storms, essential storm traits such as the rainfall duration, number and timing of peak intensity values are lost (Jetten, 2016; Lumbroso et al., 2011). Moreover, design storms are constructed from point based ground observations which are susceptible to numerous errors affecting the quality and reliability of the design storm (Qi et al., 2016; Tennant & Hewitson, 2002). In extreme events, such as with the case of TCs, ground based stations often get damaged and destroyed leading to gaps in data or underestimated rainfall totals due to the high wind speeds associated with TCs (Acevedo, 2016; Knight & Davis, 2009; Qi et al., 2016). Another disadvantage of design storms as a result of input data, is the lack of spatial variability of ground stations. Precipitation tends to vary spatially with higher rainfall amounts being observed in mountainous areas than in flat plains (Kirshbaum & Smith, 2009; Nugent & Rios-Berrios, 2018; Smith et al., 2012). In areas of limited accessibility such as areas with steep terrains, thick vegetation or over water bodies, spatial variability of rainfall is left unaccounted for (Tennant & Hewitson, 2002), limiting the reliability of using design storms in replicating flood hazard from erratic TC events.

The advancement of technology, particularly satellite precipitation measuring instruments, has resulted in a shift in the sole use of ground based measuring instruments in understanding and predicting future flood hazards, to a more broad analysis using satellite precipitation measuring instruments (F. J. Chen & Fu, 2015; Jiang et al., 2008; Lonfat, Marks Jr, & Chen, 2004). Satellite precipitation measuring instruments such as, the Tropical Rainfall Measuring Mission (TRMM) (1997-November 2014); and the NASA Global precipitation Mission (GPM) (active November 2014 to date), has shown some great advancement in analysing TC rainfall in comparison to the use of ground based stations (Huffman, Stocker, Bolvin, Nelkin, & Jackson, 2019; Landsea, Harper, Hoarau, & Knaff, 2006; Wang & Wolff, 2012). Unlike ground based stations which are constrained by distance, satellite products provide full coverage in both accessible and inaccessible areas, inland and over oceans (Jiang et al., 2008; Tan, Petersen, & Tokay, 2016; Tokay & Öztürk, 2012). The large coverage provided by satellite rainfall measuring instruments enable researchers to study the rainfall patterns, observe rainfall trends and prepare for rainfall scenarios that have not been precedented in respective study areas (Emanuel, 2017; Huffman et al., 2019; Pielke, 2005).

Despite, however, the advancements made in satellite precipitation measuring instruments, which make it possible to monitor and replicate the structure of TC rainfall (Zhou & Matyas, 2018), there still exist a strong reliance on the use of design storms (Balbastre-Soldevila et al., 2019; Lumbroso et al., 2011). One advantage of using design storms over rainfall structures extracted from satellites, is that design storms offer the possibility of associating a rainfall event with a given return period. A disadvantage, however, is that design storms are very different from actual storm events, with respect to both spatial and temporal structures (Fattorelli, Dalla Fontana, & Da Ras, 1999). Design storms tend to simplify vital storm information such as rainfall magnitude, duration, number and timing of peak intensity values, among others. The loss of essential storm information by design storms influences the results of the simulated flood hazard (Balbastre-Soldevila et al., 2019). For small uniform rainfall events, the loss of storm traits may instigate minor differences in simulated flood hazard between the design storm and the actual storm event. When dealing with extreme rainfall events, however, the simplification of storm traits by the design storm may result in major implications on the decisions made for flood mitigations owing to the differences in simulated flood characteristics between the design storm and the extreme rainfall event (Fattorelli et al., 1999).

Research objectives

This research seeks to develop a worst-case rainfall scenario from a TC event and evaluate the flood implications of simulating the worst-case TC rainfall scenario against a design storm of comparable rainfall characteristics. Where, a worst-case TC rainfall scenario is defined as an extreme rainfall pixel, from the passage of a TC, that produces the highest overall flood characteristics in comparison to other extreme rainfall pixels along the trajectory of the TC. To achieve the research objective, two objectives formulated below are used:

Objective 1: Extract and analyse extreme rainfall pixels from the passage of a TC.

RQ 1.1 What strategy can be used to extract extreme TC rainfall pixels from a TC pathway given temporal layers of satellite precipitation images?

RQ 1.2 What information can be obtained pertaining to the TC rainfall distribution from using the implemented strategy?

RQ 1.3 What are the differences in rainfall variability if the worst-case rainfall scenario is to be based on the highest magnitude or highest maximum intensity pixels?

Objective 2: Evaluate the flood characteristics between the extreme TC rainfall pixels and a design storm of comparable rainfall characteristics.

RQ 2.1: For Dominica, five design storms were created with return periods of 5, 10, 20, 50 and 100-years with different magnitudes and peak intensities (Jetten, 2016). Which design storm should be used to compare with the extracted TC extreme rainfall pixels?

RQ2.2: How do the flood characteristics of the selected design storm compare with the flood characteristics simulated from the extracted extreme rainfall pixels of the TC?

RQ 2.3: What are the implications of the flood characteristics simulated from the selected design storm and the worst-case rainfall scenario of the TC?

Research strategy

This research will make use of the 2017 Atlantic basin TC Maria. TC Maria resulted in high levels of flooding, vast damages and destructions within Caribbean islands particularly in the islands of Dominica and Puerto Rico (Barclay et al., 2019; Klotzbach et al., 2018; Schnitter et al., 2019). Although not the most destructive cyclone on record (National Hurricane Center, 2018), TC Maria is chosen because it is one of the most recent of the most destructive cyclones and hence incorporates the influence of climate change on rainfall structure. A detailed description on the development and movement of TC Maria is provided in Pasch, Penny, & Berg (2019).

The overview of the research's approach is given in Figure 1.1. First, TC Maria's rainfall characteristics will be analysed to extract extreme rainfall pixels from which a worst-case rainfall scenario will be derived. Using the selected TC extreme rainfall pixels as input to a hydrological simulation model (OpenLISEM), the flood characteristics from the extreme TC rainfall pixels will be compared against that produced by a design storm of comparable rainfall characteristics. Using the worst-case rainfall scenario, the flood implications of using the design storm or the worst-case TC rainfall scenario will be evaluated. The flood evaluations will be done for the southern part of Dominica, where TC Maria was particularly destructive, and where previous research has given vast insight into the impact of TCs (Nugent & Rios-Berrios, 2018; Ogden, 2016).

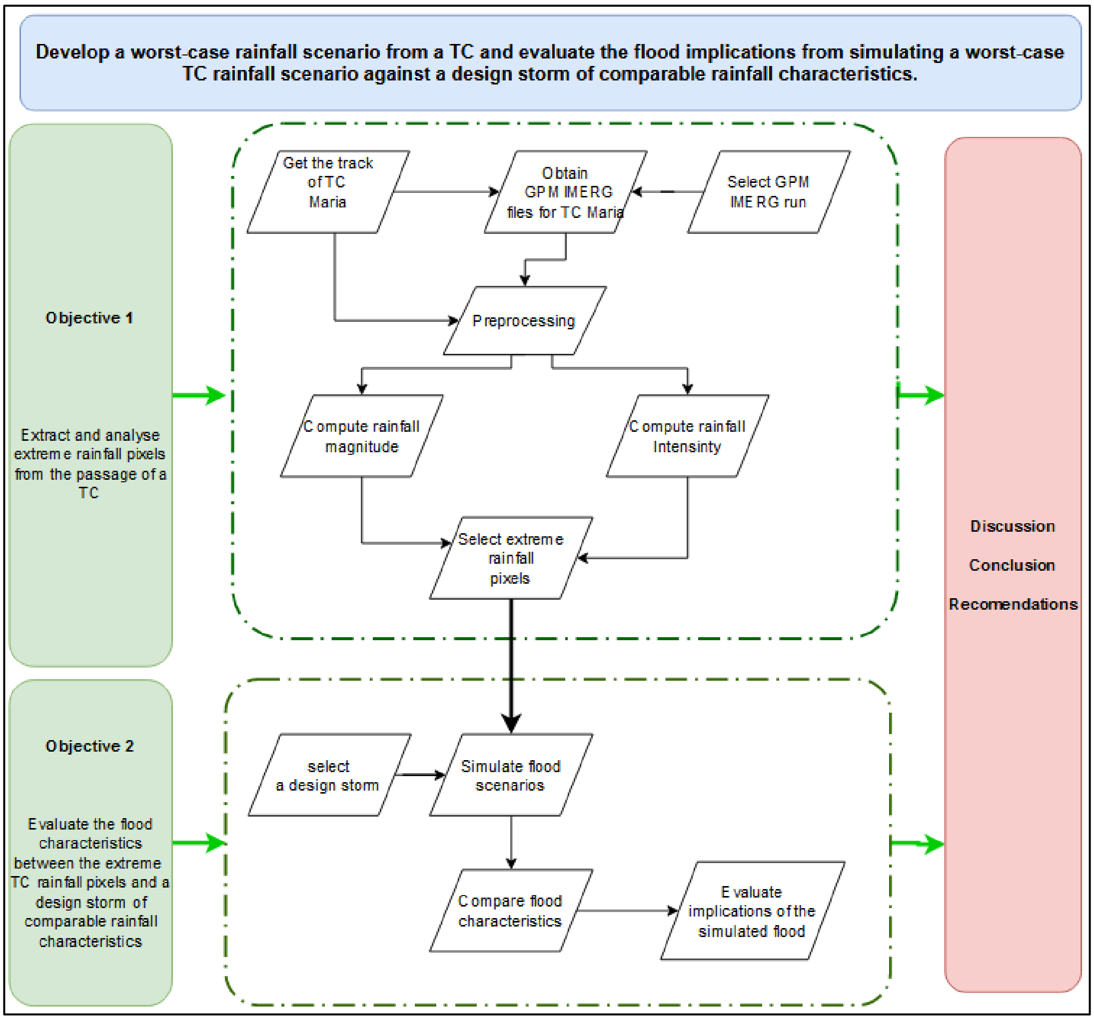

Figure 1.1: Overview of the research strategy. Upper most block states the main research objective. Extreme left blocks contain the two research objectives. The arrows are used to show the sequence of steps used in the analysis.

Research structure

This research is organised into eight chapters. Chapter one provided the background information leading to the research objectives. Chapter two will describe the study area and the datasets used in answering the above stated objectives. The methodology applied in extracting and analysing TC Maria's precipitation data and the flood modelling methodology will be given in chapters three and four, respectively. Following which, the precipitation results will be described in chapter five and the flood modelling results presented in chapter six. Discussions and conclusions of the precipitation and flood modelling results will be given in chapter seven. Finally, recommendations for future studies will be provided in chapter eight.

CHAPTER 2 STUDY AREA AND DATASETS

This research focusses on two operational scales, regional scale, and local scale. The regional scale represented by the North Atlantic Basin is used to track TC Maria and analyse the variations in rainfall intensity and magnitude along the TC's trajectory. A local scale of the southern part of the island of Dominica is used to model the flood hazard potential from extreme rainfall pixels resulting from the passage of TC Maria.

2.1 North Atlantic Basin

The North Atlantic basin constitutes of three areas; the North Atlantic ocean, the Caribbean Sea, and the Gulf of Mexico, shown in Figure 2.1 (left). Tropical cyclones within the North Atlantic basin generally evolve west Africa around 15⁰N and move west towards the Caribbean sea (Goldenberg, Landsea, Mestas-Nuñez, & Gray, 2001) were they later on veer eastwards due to Coriolis forces (S. S. Chen et al., 2006). On average, 10 tropical cyclones of over one hundred TC seedlings within the Atlantic basin reach tropical storm stage, and about six mature into severe tropical cyclones (Meteorological Department Curacao, 2015) causing significant flooding and damages to the Caribbean islands, Mexico and the US.

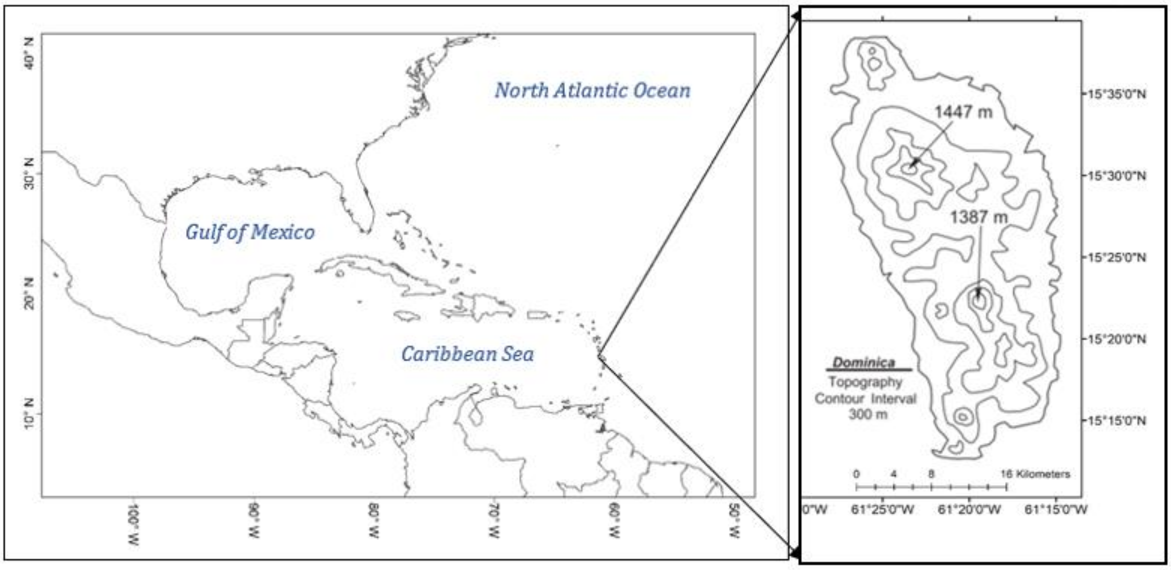

Figure 2.1: Geographical location and constitutes of the North Atlantic basin (left). Location of Dominica Island within the North Atlantic basin and the generalised 300m contour interval topographic map of Dominica (right) adopted from *Ogden (2016).*

2.2 Southern Dominica catchments

Dominica is one of the small island states within the Caribbean Sea which faces high risks of tropical cyclones. The island which is only 45km long and 23km wide has one of the most rugged terrain of all Caribbean islands (Ogden, 2016; The World Bank, 2012). The island's terrain shown in Figure 2.1 (right) exponents flood hazard posing threats to coastal areas where over 90% of the inhabitants reside. (Government of the Commonwealth of Dominica & Damage, 2015). The southern part of Dominica, which is inclusive of Dominica's largest catchment and highest populated city, Roseau, and the islands' second largest catchment, Grand Bay, is used in this study as the catchment for flood modelling. Figure 2.2 shows the extent of the southern catchment. The left side of Figure 2.2 shows the topographic information of the island whilst the right side shows the river channels and watershed boundaries within the catchment. Elevations of over 900m are found mostly at the top right corner of the island. River channels within the catchment are separated into 20 watershed areas, with channels following along the terrain of the island. The southern catchments covers a total area of 201km² with Roseau occupying 33.9km² and Grand Bay 22.5 km².

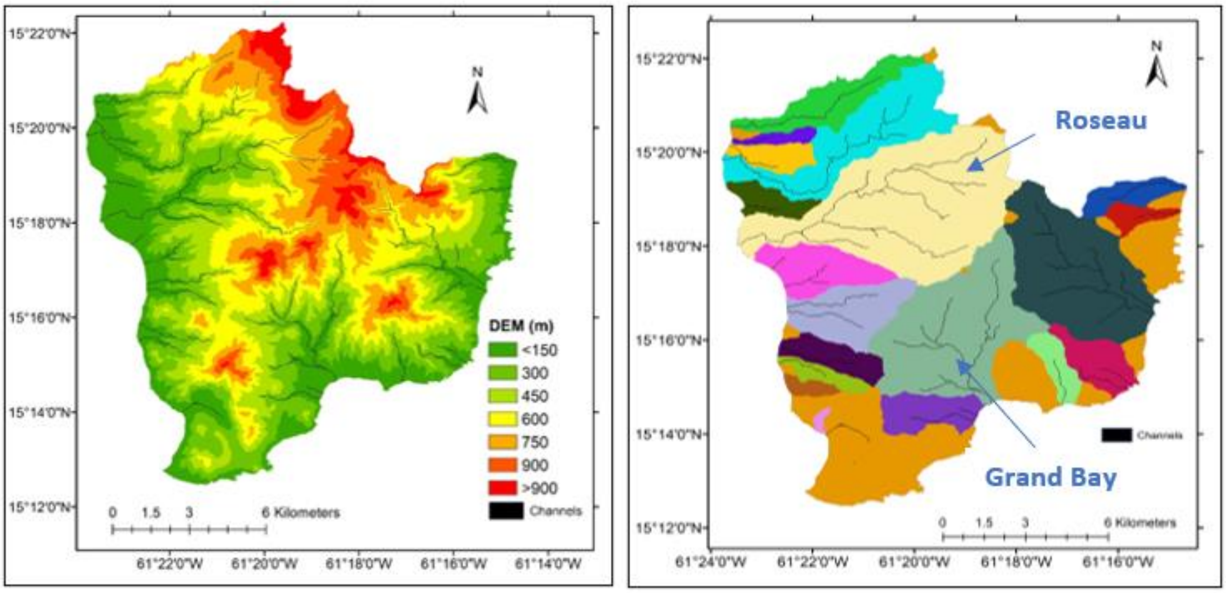

Figure 2.2: Extent of Dominica's southern catchment with the DEM (left) and sub-catchments and river channels (right).

Settlements are spread near the coastal areas owing to the terrain of the island (Ogden, 2016; The World Bank, 2012). Figure 2.3 shows the topography of the southern catchment. Highest building density is observed in the islands' capital city, Roseau. River lines follow along the terrain of the island. Several buildings are spread along the river channels as can be seen for Roseau and Grand Bay areas.

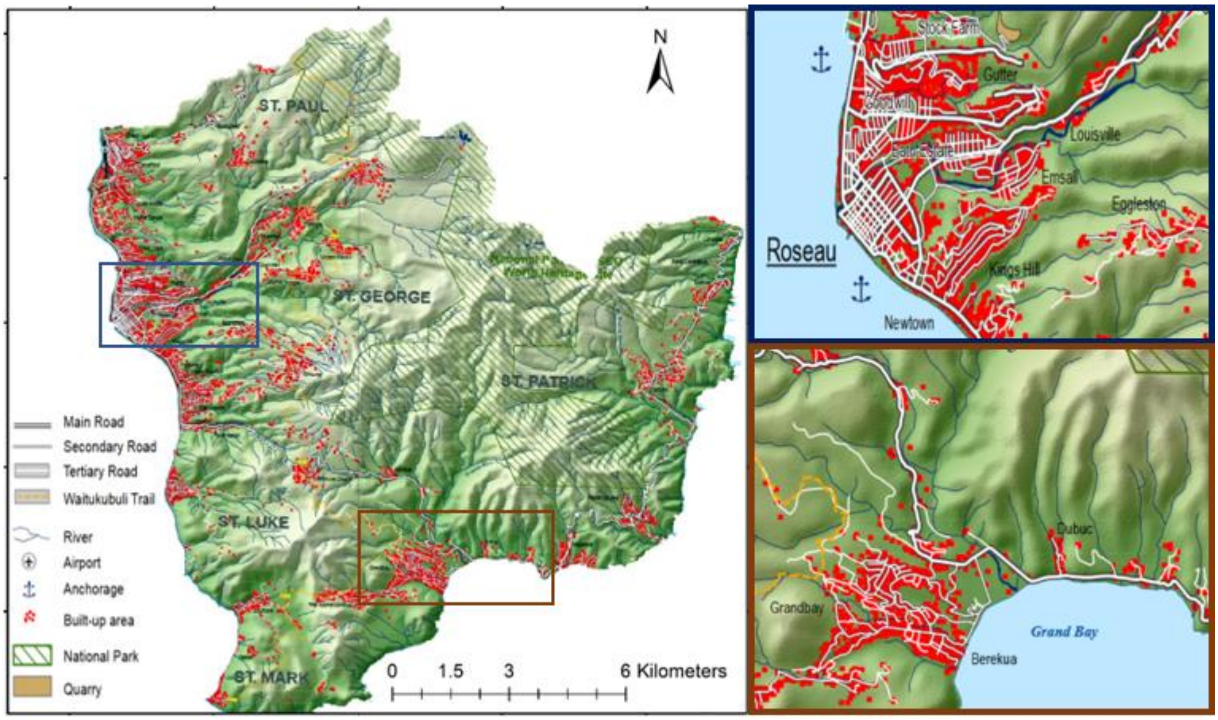

Figure 2.3: Topographic map of the Southern catchment of Dominica adopted from the 2016 CHARIM project. The right side infills show a more detailed topography of Roseau (top) and Grand Bay catchment (bottom).

For flood simulations, Dominica's base maps, were adopted internally from calibrations done on Dominica by Bastian Bout (PhD student at the time of this research). The original base maps were created during the CHARIM project by Jetten (2016), and are available from the CHARIM Geonode (http://charim-geonode.net/). Since the CHARIM project, a Lidar DEM has been constructed for Dominica, greatly improving the terrain representation. The resulting calibration variables adopted in this research are documented in Bout 2020 (in press).

2.3 Rainfall data

2.3.1 TC Maria's path

The first objective of this research is to extract and analyse extreme rainfall sections that resulted from the passage of TC Maria. To understand and analyse precipitation associated with TC Maria, data on the movement of the TC was required. The data was retrieved from the International Best Track Archive for Climate stewardship (IBTrACS) database, version 4. The IBTrACS database provides the best position of the centre of the TC's eye at a 6-hour resolution (Knapp, Kruk, Levinson, Diamond, & Neumann, 2010). In addition, the IBTrACS data includes information on the wind speed and TC category at the time of observation. Apart from being specified at 6-hour point locations, the IBTrACS dataset also provides TC category data as continuous lines along the path of the cyclone. Figure 2.4 shows the path of TC Maria and the category of the TC along each 6-hour interval. For TC Maria, the IBTrACS data covers the period the TC became a tropical depression on the noon of the 16th of September 2017 until the noon of 2nd October 2017 when the TC's maximum 1-minute wind speed became less than 30km/hr.

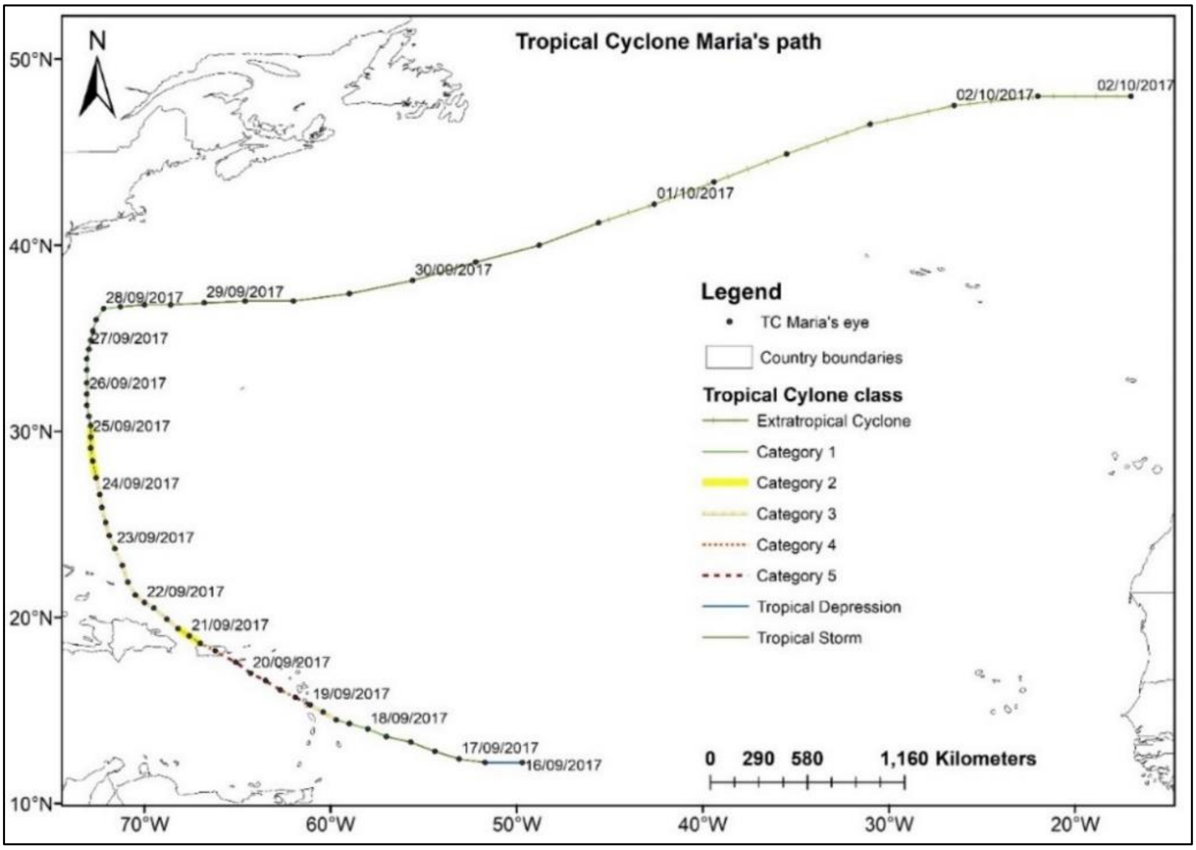

Figure 2.4: Position of TC Maria's eye, observed at every 6 hour interval from the 16th of September to the 2nd of October 2017. Lines connecting the eye positions show the interpolated path of the cyclone as well as the TC category as recorded by the IBTrACS database.

2.3.2 Satellite rainfall data

Satellite precipitation rain data for TC Maria was used to analyse the cyclone's rainfall pattern and identify extreme rainfall pixels that would be simulated against one of Dominica's design storms. The satellite precipitation data was retrieved from the Global Precipitation Measurement (GPM) Integrated Multi-satellite Retrieval for GPM (IMERG) products, within the NASA GIOVANNI platform (https://giovanni.gsfc.nasa.gov/giovanni/). IMERG products were retrieved under the current IMERG version 05. Compared to other satellite precipitation measuring instruments, GPM IMERG products provide rainfall estimates at higher spatial and temporal resolution of 0.1^{0} and 30minutes respectively between ±60^{0} latitudes (Tan et al., 2016).

GPM IMERG products are available under the early, late, and final runs with a delay of 4 hours, 12 hours and 2 months, respectively (Khan & Maggioni, 2019). The delay in precipitation estimates is owed to the correction factors applied to the runs. The GPM IMERG final run is said to provide the best precipitation estimations as it provides estimates with monthly gauge adjustments in addition to the climatological gauge calibrations applied to the early and late runs (Tan et al., 2016). However, initial comparisons of the total rainfall estimates from the IMERG final run and the National Hurricane Centre (NHC) ground observations, reported in the NHC synoptic reports, showed underestimates in IMERG final run rainfall totals. To select the best GPM IMERG run to use, comparisons were made between the three GPM IMERG runs and the NHC ground observations. The results of the comparisons given in Appendix 1 showed fluctuations in closeness values with the NHC results and hence a choice could not be made based on the comparisons. Nevertheless, personal communication between myself and NASA personal George Huffman (18.10.2019) led to the use of the GPM IMERG final run as the satellite precipitation dataset for this research. Appendix 1 provides the details leading to the selection of the GRM IMERG final run dataset.

2.3.3 **Ground based rainfall data**

To decide on which GPM IMERG product run to use for TC Maria's rainfall analysis, ground based rainfall data was required to compare with rainfall estimates from the GPM IMERG runs. The ground rainfall data was retrieved from the National Hurricane Centre (NHC) tropical cyclone synoptic reports. The rainfall data was available as estimates of the total rainfall obtained from the passing of a tropical cyclone. The ground rainfall estimates were given with a generalised description of the location of the ground-based stations, for instance, over 330mm recorded in the south west part of Cuba. Ground-based rainfall estimates from NHC synoptic reports were retrieved for two TCs; 2016 TC Matthew (Stewart, 2017) and 2017 TC Maria (Pasch et al., 2019). TC Matthew was used in this case to investigate possible consistencies in the differences between the GPM IMERG product run and the ground-based rainfall data.

2.3.4 **Design storm**

To compare the flood characteristics that would result from the worst-case rainfall scenario of TC Maria and what is used for flood hazard assessments, Dominica's design storms had to be used. The design storms were adopted from the 2016 Caribbean Handbook on Risk Information Management (CHARIM) project. The adopted design storms were created in two steps. First, a Gumbel analysis was done on the daily rainfall for Dominica's two stations with records from 1975. Second, design curve shapes were computed from 5-minute rainfall estimates, observed from 15-20 functioning tipping buckets over a period of 12 years in St Lucia, an island in the south of Dominica with similar physiography. To scale the design curve shapes to Dominica's magnitude, the 5, 10, 20, 50 and 100-year Gumbel analysis computed from daily rainfall records from Dominica's two stations were used. Figure 2.5 shows the rainfall characteristics for Dominica's design storms that have been adopted in this research. The design storms show higher peak intensity values to decrease with an increase in rainfall magnitude. A detailed description of the creation of Dominica's design storms is found in Jetten (2016).

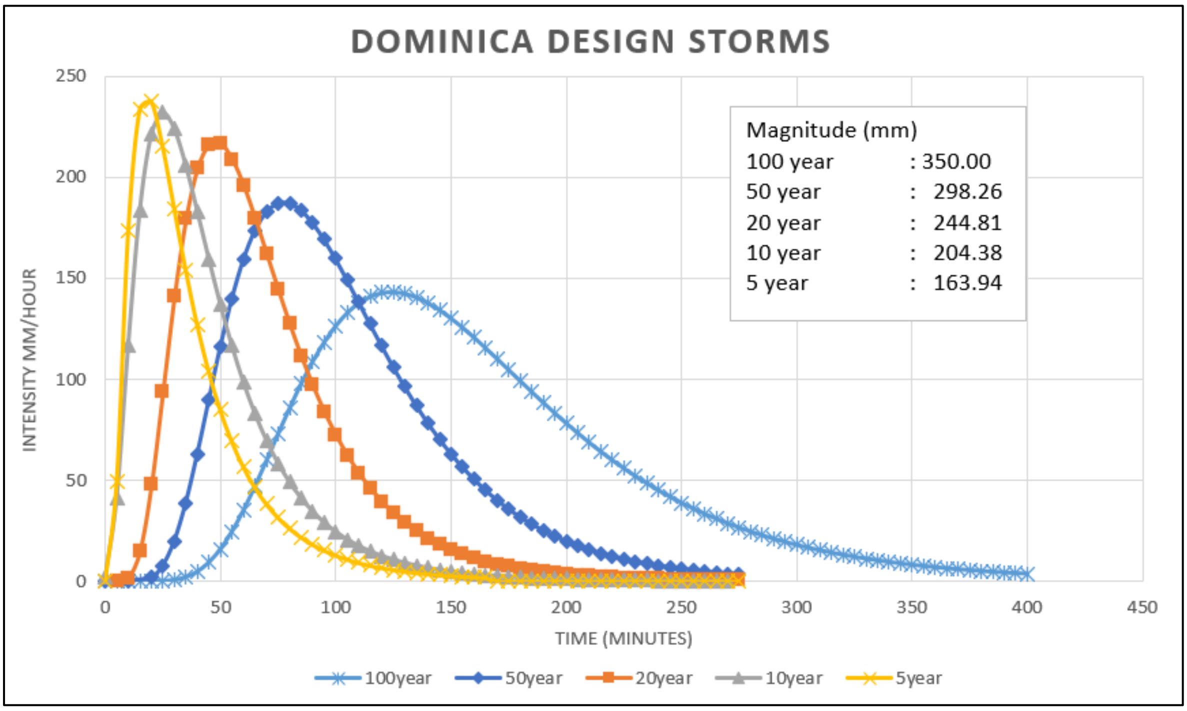

Figure 2.5: Dominica's 5, 10, 20, 50 and 100-year design storms adopted from the CHARIM project. Source *(Jetten, 2016)*.

CHAPTER 3 RAINFALL ANALYSIS FOR TC MARIA

To extract extreme rainfall pixels of TC Maria, the IBTrACS and GPM IMERG datasets needed to be pre-processed and the TC's statistical variables, magnitude, and intensity, quantified.

3.1 Pre-processing of the IBTrACS and GPM IMERG datasets

Data prepossessing and analysis was done using ArcMap version 3.1.0 and R version 3.6.1 (*05.07.2019*) The WGS 84 coordinate system was adopted as the base coordinate for all spatial data used in this research. The pre-processing of the GPM images had to be done before the precipitation characteristics associated with TC Maria could be computed. The pre-processing was done in three steps which are explained under I – III below.

I. Positioning TC Maria on each GPM Image

The position of TC Maria's eye, retrieved from the IBTrACS dataset, needed to be matched to the IMERG precipitation data to obtain the location of TC Maria's eye in every precipitation image. Given the differences in the temporal resolution of the IBTrACS and IMERG datasets, linear interpolation was used. This method was adopted from Zhou & Matyas (2018), who matched the IBTrACS temporal resolution to the 3-hour TRMM data. Interpolating TC Maria's eye positions resulted in 769, 30minute location data of TC Maria's eye for the duration of the cyclone.

II. Eliminating non-TC related precipitation

This research was solely interested in precipitation associated with TC Maria, whereas precipitation may occur in nearby areas independent of the TC. For this reason, it was essential to eliminate all non-TC related rainfall prior to further analysis. Figure 3.1 shows the GPM IMERG precipitation estimate on the 16th of September 2017 between 12:00:00 -12:29:59 when the first TC Maria's eye position was recorded by the IBTrACS database. Rainfall is observed to have occurred along and near the path of TC Maria independent of the TC. To eliminate all non-TC related rainfall, 500km radiuses for each 30-minute eye position of TC Maria were used to define the maximum extent of the TC rainfall for each precipitation estimate. The 500km radius value was obtained from previous studies which investigated TC related rainfall (Agustín Breña-Naranjo, Pedrozo-Acuña, Pozos-Estrada, Jiménez-López, & López-López, 2015; F. J. Chen & Fu, 2015; Lonfat et al., 2004; Ramos-Scharrón & Arima, 2019). A total of 769 buffered precipitation images, corresponding to the date, time and location of TC Maria were extracted.

III. Equalising the processing extent

To allow for automatic analysis in R, the extracted images (part II of Section 3.1) had to be set to the same spatial extent. The spatial extent, defined by four sets of longitude and latitude values (bounding box coordinates), varied due to the progression of the TC. To equalise the spatial extent, a raster base map was created in ArcMap which covered the extent of TC Maria's path. The values of the raster base map were set to zero. The extracted precipitation images were individually added to the raster base map creating 769 precipitation images with the same spatial extent.

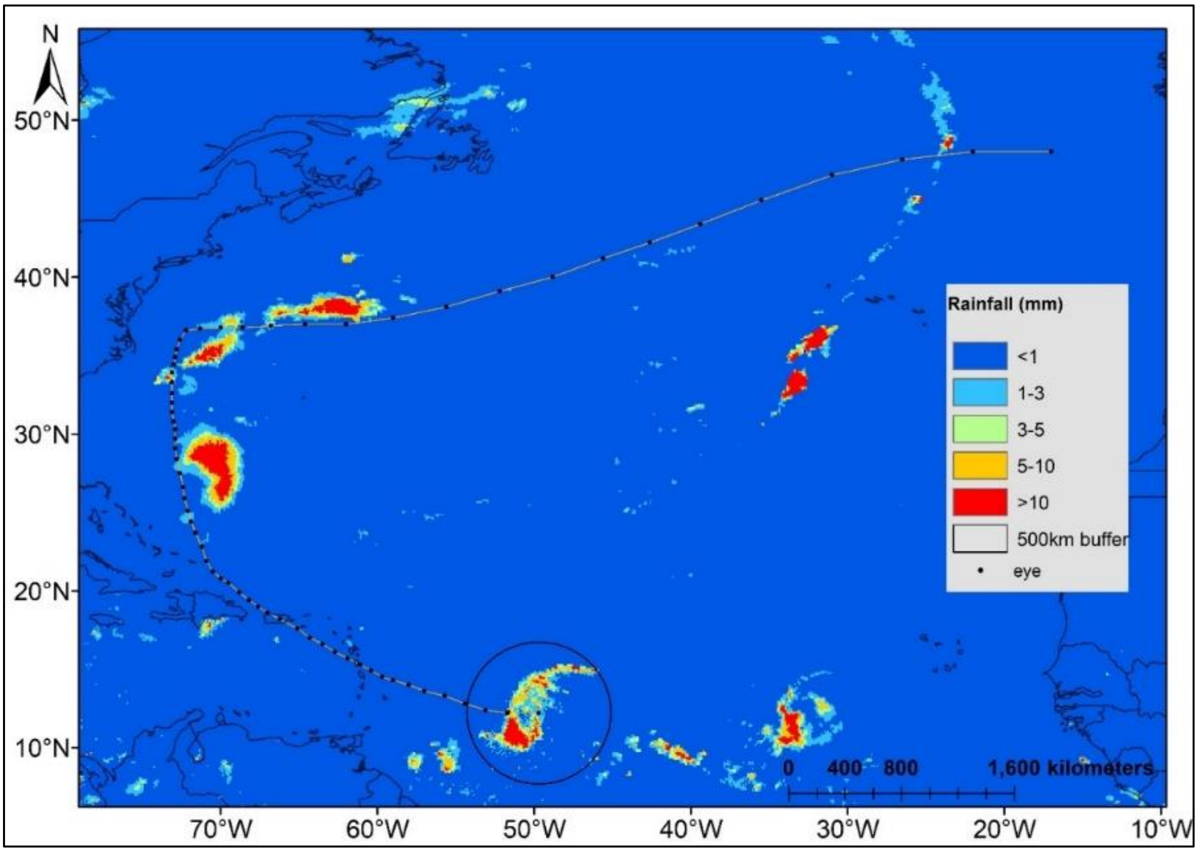

Figure 3.1: Precipitation estimates from the GPM IMERG final run, observed on the 16th of September 2017 between 12:00:00 and 12:29:59 when the centre of TC Maria's eye is at the first point of observation. Rainfall associated with TC Maria at the time of observation is bounded by the 500km buffer.

3.2 Analysing the precipitation characteristics of TC Maria

Using the GPM pre-processed images (as described in part III of Section 3.1) computations were made for rainfall variables, magnitude and intensity. TC rainfall magnitude is defined in this research as the total amount of precipitation per pixel associated with the overpass of TC Maria, independent of its duration. Correspondingly, the rainfall intensity will be defined as the hourly rainfall average per pixel associated with the overpass of TC Maria. Section 3.2.1 and Section 3.2.2 provide a description of the methodology applied in computing TC Maria's magnitude and intensity values, respectively.

3.2.1 Magnitude

Since this research seeks to analyse flood characteristics from extreme rainfall pixels, there was a need to extract high rainfall magnitude pixels from TC Maria so as to provide rainfall input scenarios for flood modelling. Computations for rainfall magnitude were done by developing an R script (see: Appendix 2) that stacked and summed the 769 pre-processed GPM images (part III of Section 3.1) to get the magnitude values per pixel for the duration of TC Maria. In R, a boxplot was then used to visualise the spread of the magnitude values. From the boxplot upper-class, a threshold value was defined by considering the size of the differences between consecutive magnitude values. For each selected magnitude, time series plots were made ranging from the first to the last non-zero value recorded in each pixel. An analysis of the time series plots, magnitude and intensity values, allowed for the selection of magnitude scenarios that would be modelled for flood analysis. For each selected magnitude scenario, distances were computed from the position of TC Maria's eye at the time of the recorded rainfall intensity value, to the centre of the pixel with the selected scenario. The distance computations were done to observe the development of the time series in relation to the position of the cyclone.

3.2.2 Intensity

Apart from floods resulting from large rainfall magnitudes, high rainfall intensity values prompt flash flooding even when low magnitudes are involved (Beguería, Vicente-Serrano, Lopez-Moreno, & Gracia-Ruiz, 2009). For this reason, analysing TC Maria's maximum rainfall intensities was essential. In R, code lines were added to the developed script explained in section 3.2.1 (attached in Appendix 2), to plot the maximum intensity values from each of the GPM pre-processed images. The maximum intensity plot gave an indication of the maximum intensities observed within a 500km TC's eye radius for each precipitation image. Using the maximum intensity plot as a guideline for the range of intensities, a threshold value was assigned to select pixels with the highest intensity values. Similar to the method applied for selecting magnitude scenarios (section 3.2.1), time series plots for the highest intensity pixels were made, and their magnitude and intensity values used in selecting high intensity scenarios. For the selected scenarios, distances were computed from the centre of the selected pixels to the position of TC Maria's eye at the time the plotted intensity value was recorded.

3.3 Comparative analysis of selected rainfall scenarios

Before comparisons can be made on the flood characteristics of selected pixels of TC Maria and a comparable design storm (objective 2), the differences in the rainfall characteristics had to be analysed. Analysis on the differences in rainfall characteristics were done using cumulative rainfall plots. The cumulative rainfall plots were made for the entire duration of TC Maria's rainfall on a pixel, regardless of the intensity value. Likewise, the cumulative plot of the design storm considered the entire rainfall duration of the design storm as is given in the CHARIM project.

CHAPTER 4 FLOOD MODELLING

The second objective of this research is to evaluate the flooding characteristics between the extreme TC rainfall pixels of TC Maria against a comparable design storm, for the southern part of Dominica.

4.1 OpenLISEM

The modelling process was done using the Open Source Limburg Soil Erosion Model (OpenLISEM). OpenLISEM, interchangeably referred to as LISEM, is an event based, spatial hydrological and soil erosion model that simulates rainfall runoff, sediment deposits and shallow floods on small catchments (Starkloff, Stolte, Hessel, Ritsema, & Jetten, 2018). LISEM has been applied in a number of studies in simulating sediment deposits (Grum et al., 2017) and surface runoff (de Barros, Minella, Dalbianco, & Ramon, 2014; Gomes, Mello, Silva, & Beskow, 2009) and has proven successful in both sedimentary and hydrological processes. As the purpose of this study is to simulate floods, only the hydrological part of the model was used. Figure 4.1 gives a conceptualised view of the hydrological simulations in LISEM.

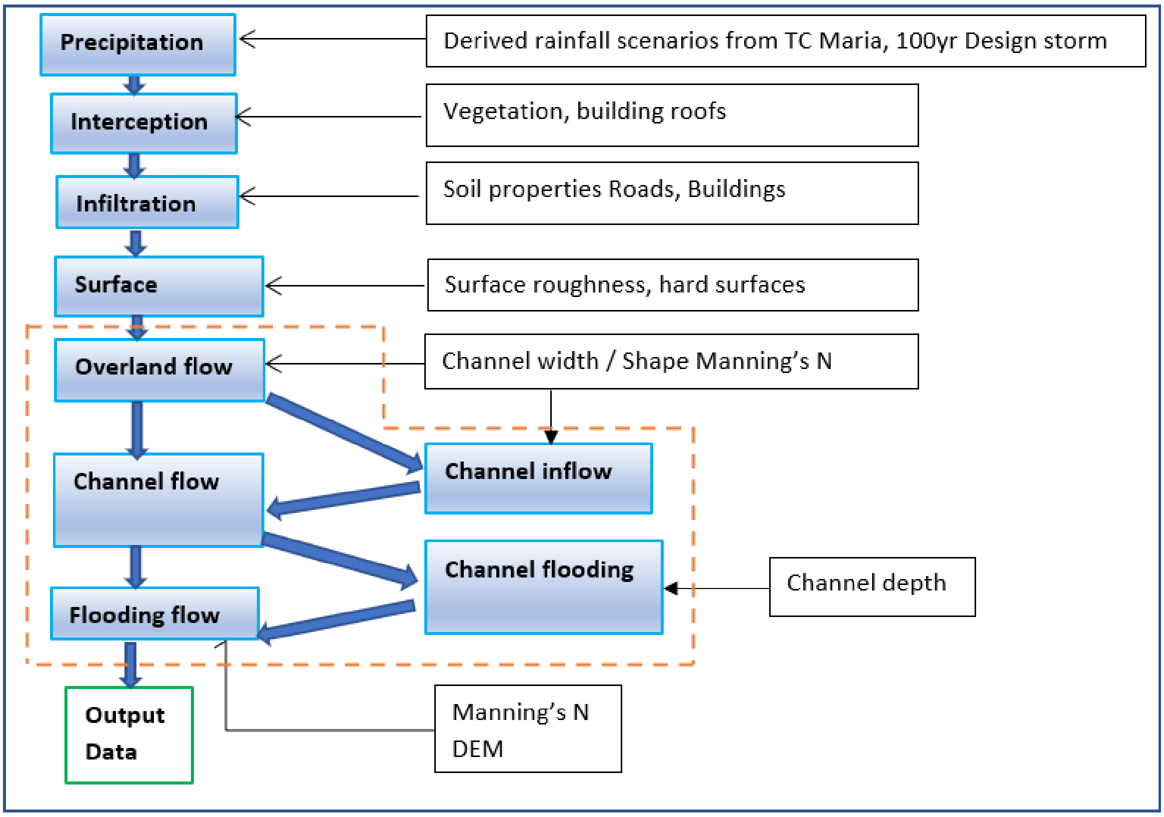

Figure 4.1: An overview of the order of LISEM's hydrological simulations. The main processes are shown in blue boxes and the example input files are given in the white boxes. The fragmented red box shows the order in which the actual flood occurs. Adopted from *(Bout and Jetten 2018)*

4.2 Model setup

Three surface flow options are available in LISEM. (I) the 1D Kinematic Wave for overland flow using surface drainage direction network (no flooding), (II) 1D kinematic overland flow and 2D dynamic flood from overflowing channels, and (III) 2D dynamic wave for overland flow and flood (using the DEM). For this research, option (II) was used. The flow option was chosen because it allows for flood to be observed from the overflowing of channels as is the case with Dominica, where the islands' terrain poses great influence to the propagation of the floods (Ogden, 2016). Figure 4.2 shows a detailed order of the flow processes (fragmented red box in Figure 4.1) as is routed by the DEM for water balance computations in LISEM. In the first process (1D hydrology), a subtraction is done on the precipitation intercepted by vegetation canopy and building roofs. The remining precipitation which reaches the surface is then infiltrated depending on the surface properties and soil capacity. For process 2 (1D/2D runoff), the runoff flows on the surface along the predefined flow network. In process 3 (1D discharge wave), the runoff fills river channels and causes a rise in discharge. 2D flooding begins at process 4 when the river water exceeds the channel capacity. Process 5 shows flood recession which occurs after rainfall and runoff process have stopped. The full explanations and water balancing equations used by LISEM for the 5 processes are found in Bout and Jetten (2018). Flood simulations for this research were done using LISEM version 5.98beta (*16.03.2020*). To ensure consistence in LISEM results and numerical stability, the hydrology simulation time step was held constant at 20 seconds for all rainfall input scenarios. The base input maps adopted from Bout 2020 (in press) were resampled to a 20-meter resolution for accurate representation of the DEM.

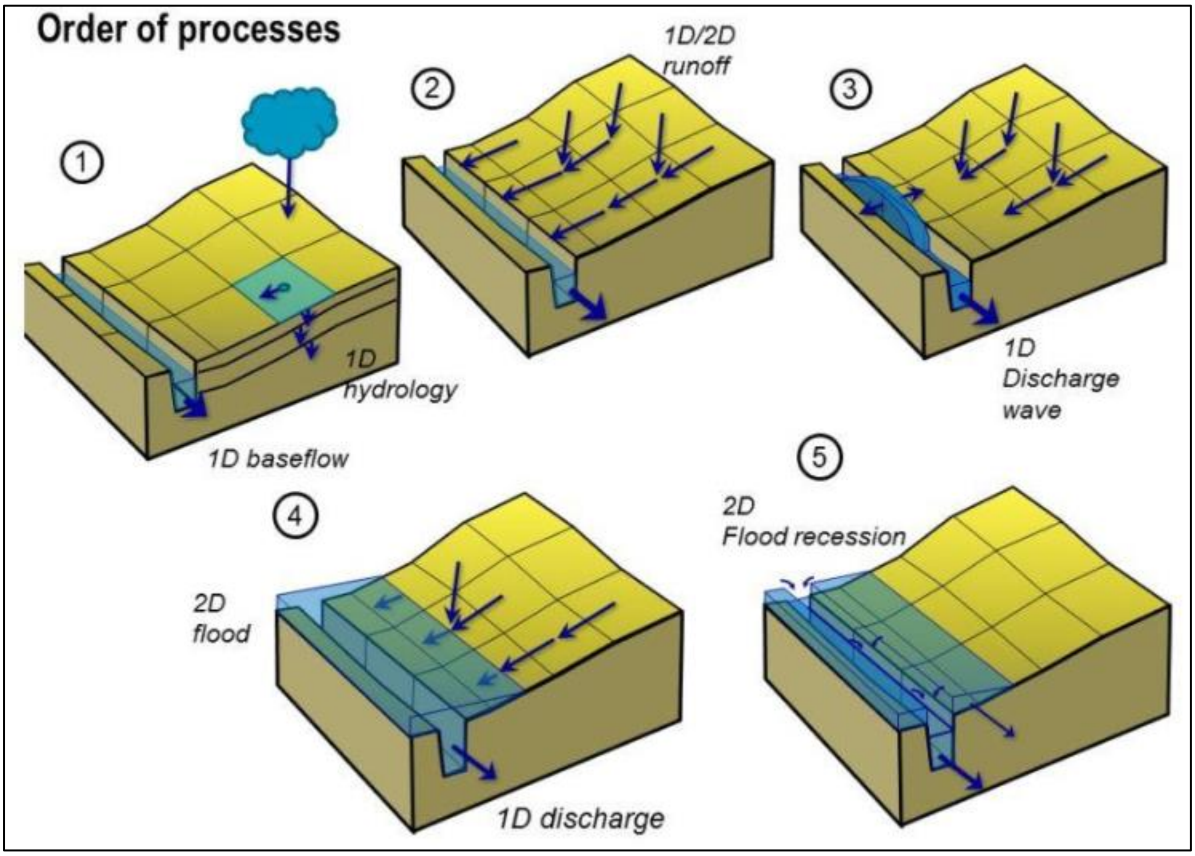

Figure 4.2: Order of flow processes as simulated by the 1D kinematic overland flow and 2D dynamic flood from channel option in LISEM. Source *(Bout and Jetten, 2018)*

4.3 Input database

OpenLISEM uses a set of spatial input data layers to simulate hydrological processes (Jetten, 2016). Figure 4.3 shows the data layers and flow chart of the creation of LISEM's input database. Three stages are implemented to narrow down the basic input maps into hydrological variables that can be understood by the model. Stage 1 shows the basic maps (Rainfall, DEM, Soil units, Land use/cover and infrastructure) needed for the catchment. Stage 2 shows detailed information about the basic maps given in the first stage. Stage 3 highlights the hydrological variables computed from the detailed information provided in stage 2 and used as the input database for OpenLISEM. In the run file, stage 4, the desired run options such as time step, start time, surface flow options, initial soil moisture, minimum flood height etc. together with the desired output map names are specified. The run options used for LISEM are stated along different sections in this chapter and attached as a summary in Appendix 3.

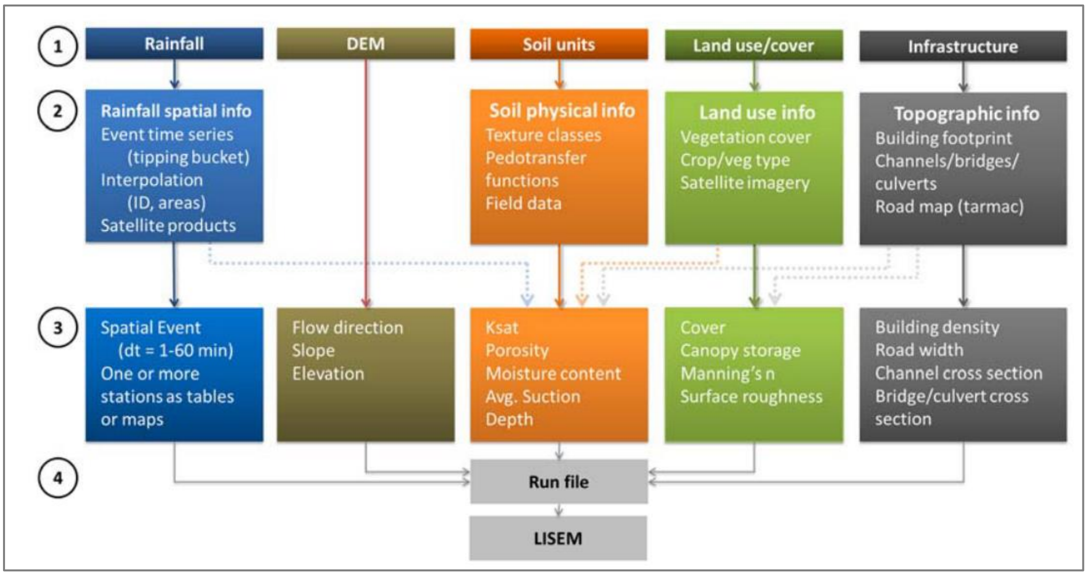

Figure 4.3: Spatial input maps used in LISEM to simulate hydrological processes. Adopted from *Jetten (2016).*

4.4 Rainfall input

Rainfall is one of the basic maps needed to simulate a hydrological process (Jetten, 2016). In this research, two classes of rainfall input scenarios are used. The first-class comprises of TC scenarios selected from analysing the rainfall characteristics of TC Maria (Chapter 3). The TC rainfall scenarios are made up of one pixel per scenario, simulated homogenously over the study area. A single pixel is used due to the relatively small difference in spatial resolution between the study area (15km by 14km, at the catchments' longest and widest cross sections) and the GPM IMERG precipitation files (11km by 11km). The second class of rainfall input scenarios contains Dominica's 100-year design storm described in section 2.3.4. The 100-year design storm was selected based on its closer resemblance in rainfall characteristics with the TC scenarios (results presented in the next chapter) as compared to the 5, 10, 20 and 50-year design storms.

4.5 Transposing the TC rainfall pixels over Dominica

Although it is well known that topography has a major impact on rainfall (Kirshbaum & Smith, 2009; Smith et al., 2012), the correction factor needed to adjust the cyclones' rainfall is not constant and is difficult to isolate from the complex mixture of processes that influence TC rainfall (Houze et al., 2017; Kirshbaum & Smith, 2009; Nugent & Rios-Berrios, 2018). To avoid diverting the research into evaluating possible orographic influences on the island of Dominica, the obtained GPM precipitation estimates are not adjusted for orographic effects.

4.6 Computing flood characteristics

TCs can produce rainfall that ranges from a few minutes to several days on a single area (Begueria et al., 2009). Low rainfall intensities (< 2mm/hr) from TC can make up for a significantly large part of the TC duration (Zhou & Matyas, 2018). Accounting for the entire TC rainfall duration means an increase in simulation time without any added advantage to the quality of the simulation results. For this research, the beginning and end time steps were set to include intensity values >2mm/hr. To compensate for the exclusion of initial light rainfall, the model was set to an initial soil moisture of 85% porosity for all scenarios modelled. The high soil moisture value meant a reduction in soil storage capacity which would compensate for the earlier rains. Apart from spatial patterns, four parameters, flood start time, maximum flood height, total flood volume and flood extent, were used to compare the resulting flood characteristics from the simulation. It is worth noting that, although the simulation is made for the southern catchments of Dominica, only Roseau and Grand Bay catchments are used to highlight the differences in the flood characteristics. The flood characteristics of the two catchments are compared separately due to the differences in catchment properties (section 2.2).

4.6.1 Flood start time

Flood start time is defined in this research, as the time at which a flood depth of over 0.05 meters, is recorded from the start of the simulation at every pixel. The depth of 0.05m is chosen to avoid spurious information of flooded areas of only a few mm or cm depth. The 0.05m value was decided in a discussion with stakeholders during the CHARIM project, as the flood depth that was completely harmless (Jetten 2020, Personal Correspondence). As addressed in the previous section, the simulation times for the rainfall scenarios were set to start when the rainfall intensity values were approximately 2mm/hr, to avoid hours of simulating light rainfall. The resulting flood start times in this research will thus be reported from the start on the simulation and not from the time the first non-zero rainfall value is recorded.

4.6.2 Maximum flood height

Flood height is an important parameter in flood hazard mapping (S. N Jonkman, Vrijling, & Vrouwenvelder, 2008; Sebastiaan N. Jonkman, Maaskant, Boyd, & Levitan, 2009). The maximum flood heights for the rainfall input scenarios were obtained from LISEM output maps. The maximum flood height classes were uniformly classified for easy comparisons between rainfall scenarios. In addition to the flood height map classifications, the differences in flood height characteristics were analysed by looking at the flood extent per flood height class and flood volume per flood height class.

4.6.3 Flood volume

In this research, the maximum flood volume refers to the total amount of water with a depth of > 0.05 meters within the catchment. For quantifiable comparisons, flood volume for the five rainfall scenarios were computed per flood height class. The percentage flood volume were computed for each rainfall scenario as the flood volume per flood height interval over the total flood volume simulated within the catchment. Since the research is focused on analysing the flood hazard from extreme rainfall events, a flood height threshold of 0.5 meters was used for the flood height classes.

4.6.4 Flood extent

Similar to flood volume, the maximum flood extent for this research was defined as the total area with a flood height > 0.05meters. The analysis of the flood extent was done using maximum flood height maps obtained as an output from OpenLISEM. Similar to quantifications done for the flood volume, flood extent was computed per flood height class using the 0.5meter flood threshold. Although the flood simulations were done for the entire southern catchment, the Roseau and Grand Bay catchments were used for detailed comparison between the five rainfall scenarios. The pc raster equations used for computing the flood volume and flood extent per flood height class (see: Appendix 4) were obtained internally from Professor Doctor Victor Jetten.

4.7 Evaluating the flood implications from the worst-case rainfall scenario and the selected design storm

The aim of this research is to develop a worst-case TC rainfall scenario and evaluate the flood implications from simulating the worst-case TC rainfall scenario against a design storm of comparable rainfall characteristics. The worst-case rainfall scenario was taken as the extreme TC rainfall pixel that produced the highest overall flood characteristics of the simulated TC scenarios. By comparing the flood characteristics of the worst-case rainfall scenario and the design storm, the implications of using either of the two approach for simulating flood characteristics were evaluated.

CHAPTER 5 GPM PRECIPITATION RESULTS

The GPM precipitation results are presented in line with the methods applied in the rainfall analysis of TC Maria (Chapter 3).

5.1 Rainfall magnitude

The summation of TC Maria's pre-processed precipitation images (section 3.2.1) gave the total rainfall per pixel as estimated by the GPM IMERG final run, for the duration of each pixel within a 500km radius of TC Maria's eye. Figure 5.1 shows the spatial distribution of the magnitude values associated with TC Maria in relation to the cyclone's category (shown in greater detail in Figure 2.4).

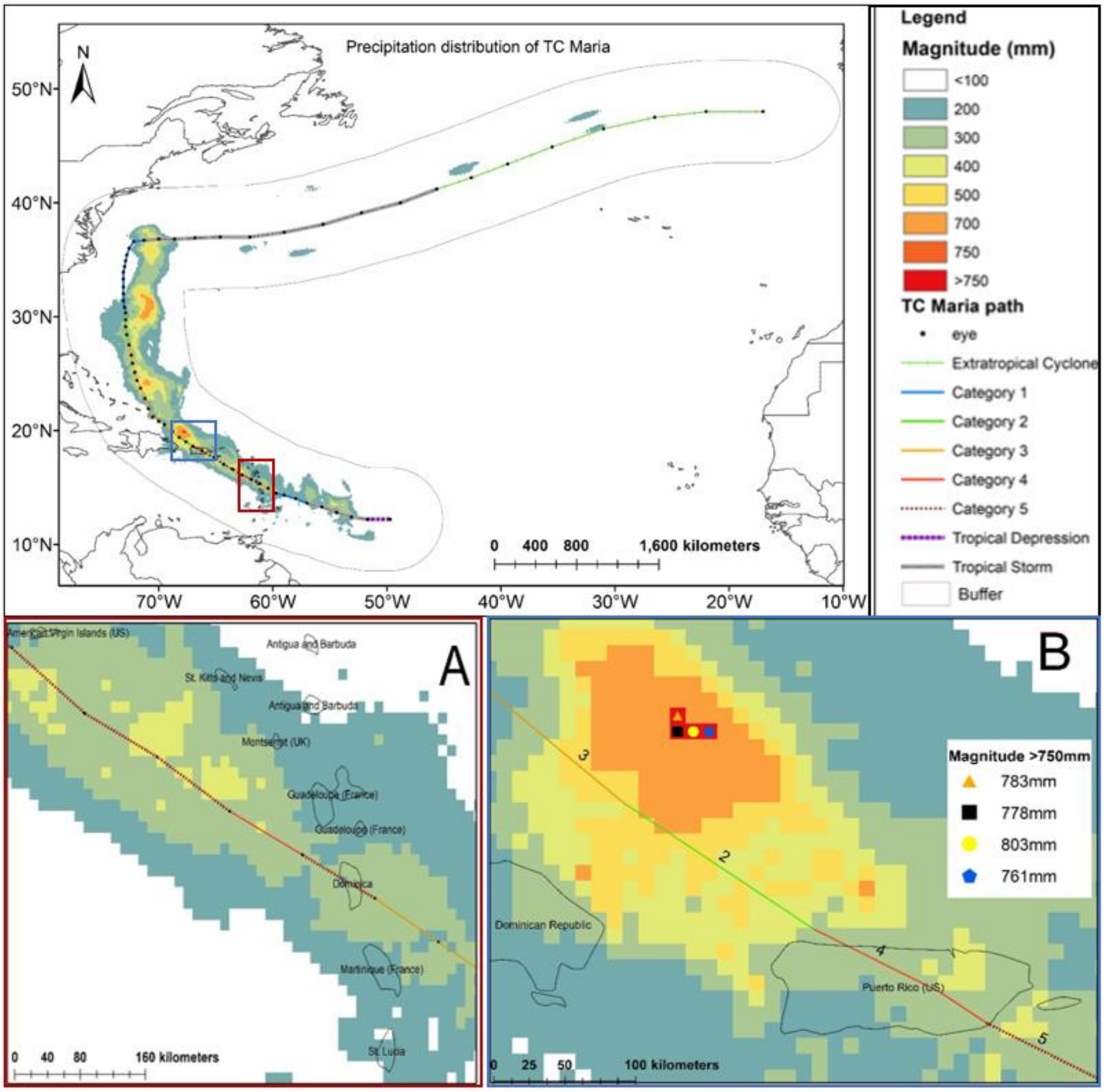

Figure 5.1: Spatial distribution of TC Maria's rainfall magnitude [mm] estimated from the GPM IMERG final run. The buffer shows the 500km rainfall extent considered in the analysis. Inserts A and B show in greater details, the rainfall distribution of the pixels surrounding Dominica and Puerto Rico islands, respectively. In addition, insert B shows the spatial distribution of pixels with magnitude values higher than 750mm observed within the entire path of TC Maria.

The occurrence of high magnitude values is seen to follow a wave like pattern. Magnitude values >700mm are observed, over the Caribbean Sea, in three distinct locations. (i) shortly after Puerto Rico, as the TC intensifies from a category 2 to a category 3 cyclone. (ii) North of Dominica Republic, during which the cyclone is a category 3, and, finally, (iii) east of USA Florida, when the TC de-intensifies from a category 2 to a category 1 cyclone. In each of the three locations, the highest magnitude pixel values occur in the centre of a cluster, surrounded by decrementing magnitude values moving away from the cluster's midpoint. On land, the computed magnitude estimates show pixel values to be lower than that observed over the Caribbean Sea. Islands such as Guadeloupe, Martinique and St Lucia (insert A of Figure 5.1) show rainfall magnitudes values from TC Maria to be less than 300mm per pixel. The islands of Dominica and Puerto Rico where TC Maria made a direct hit, show highest magnitude values of less than 500mm and 700mm, respectively. Overall, the lowest rainfall magnitude values from TC Maria are observed to have occurred when the TC moved at a higher speed, depicted by the distance between the successive 6hr TC eye positions. The low magnitude values resulted as an indication of the minimal duration of a pixel within the 500km buffer.

To select high magnitude pixels for analysis (section 3.2.1), a magnitude threshold value of 750mm was used. This threshold value was chosen to limit the analysis to four pixels as a proof of concept. The spatial distribution of the four pixels with magnitude values higher than 750mm is shown in insert B of Figure 5.1. The four pixels over the threshold value, had magnitude values of 783mm (orange triangle); 778mm (black square); 803mm (yellow circle) and 761mm (blue pentagon). For easy referencing of the pixels, aliases A, B, C and D, given according to the order in the prior sentence and following the order of the pixel arrangements (top left pixel to bottom right pixel) will be used. The four pixels (A, B, C and D) are analysed in more detail in the next section to select pixels to be used as rainfall input scenarios for flood modelling (second objective).

5.1.1 Time series analysis of the highest magnitude pixels

Next to spatial analysis of maximum magnitude pixels, time series analysis provides structural information of the TC in time. Time series plots, shown in Figure 5.2, were made for the four pixels with magnitude values higher than 750mm. Colour coding and aliases given to the pixel locations in insert B of Figure 5.1 is coordinated to the time series plots in Figure 5.2. The time series plots of the pixels with rainfall magnitude values >750mm, show structural similarities which are more evidenced for adjacent pixels (insert B Figure 5.1). Pixels C and D depicted by the yellow circle and blue pentagon in Figure 5.1 show similarities in the time series plots in Figure 5.2. Similarly, pixels A and B depicted by the orange triangle and black square in Figure 5.1 show similarities in time series plots in Figure 5.2. Adding to the structural similarities of the pixels, the time series plot also shows similarities in the time at which the first non-zero rainfall estimate are observed. Pixels C and D show similar rainfall start time as do pixels A and B.

When analysing the time series of the selected pixels, pixel C with the highest overall magnitude value (803mm) shows a lower maximum intensity (80mm/hr) as compared to pixel A with the second highest magnitude value (783mm/hr). Pixel A shows a maximum intensity value of 88mm/hr which is the highest overall intensity amongst the selected high magnitude pixels. Since the highest magnitude pixel does not have the highest intensity amongst the high magnitude pixels, both pixels A and C are selected as rainfall input scenarios for flood modelling. The two pixels, referred to from here on after as; MAG-1 and MAG-2; marks pixel C with the highest overall magnitude (803mm) and pixel A with highest intensity value amongst the highest magnitude pixels (783mm), respectively.

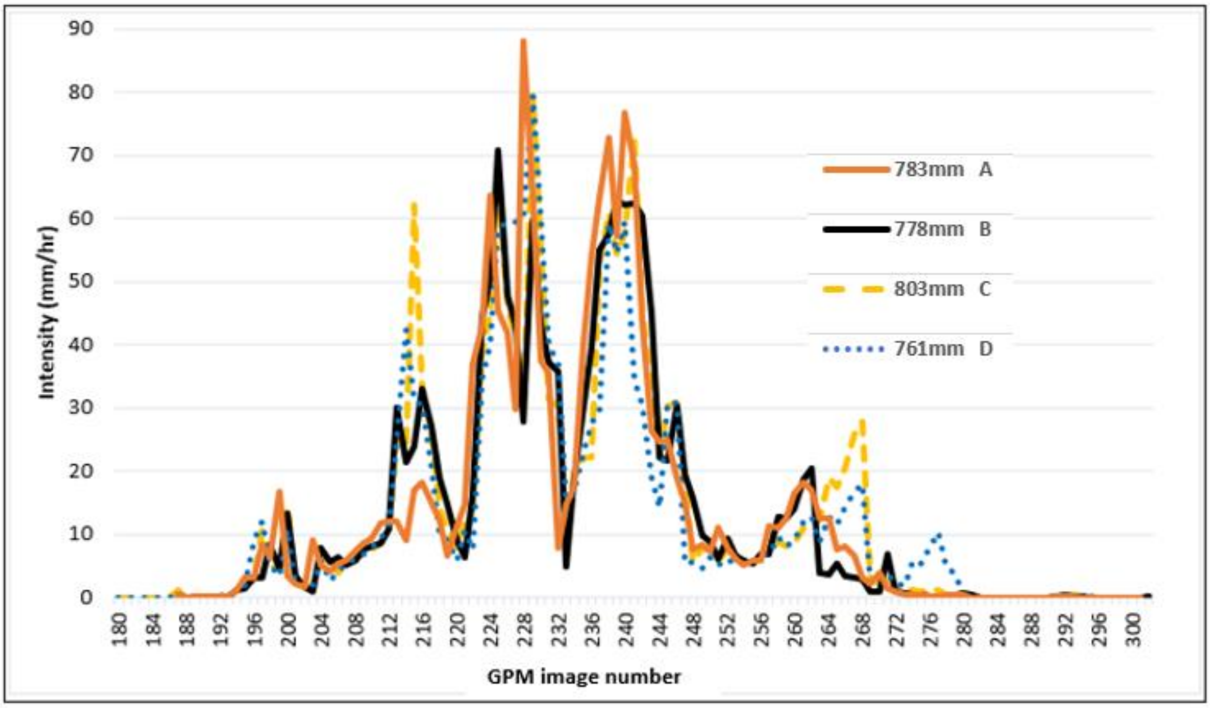

Figure 5.2: Time series plots for pixels with magnitude values higher than 750mm shown in Figure 4.3. The rainfall intensities are plotted against the observation image number at which the first to the last non-zero intensity values are observed.

Apart from differences in magnitude and intensity values, MAG-1 and MAG-2 show differences in number of peaks, rainfall duration and the time at which the first peak intensity values are observed. Figure 5.3 shows the time series plots of the two magnitude scenarios, MAG-1 (left) and MAG-2 (right), plotted against the distance between TC Maria's eye and the centre of each scenario's pixel at the time an intensity is plotted. Furthermore, Figure 5.3 gives the category of TC Maria at the time of the observed intensity value as given by the IBTrACS path data (section 2.3.1). Analysing the development of the timeseries (Figure 5.3), MAG-1 shows the first non-zero rainfall intensities from TC Maria to have been recorded when the TC's eye was approximately 400km away from the pixel's centre. The last non-zero rainfall intensity value associated with TC Maria was recorded 60 hours after observing the first rains, when the centre of TC Maria's eye was about 495km away from the pixel. On overall, intensity values > 2mm/hr for MAG-1 are observed when the centre of TC Maria's eye is less than 300km away from the pixel's centre. MAG-1 shows five major peaks (intensity >40mm/hr) to have occurred when TC Maria's eye was between 50km-150km away from the centre of MAG-1's pixel. The five peaks in MAG-1 were observed between hour 14, after TC Maria de-intensified from a category 4 to a category 2 cyclone, and hour 34 when the cyclone was a stable category 3 cyclone. The highest peak intensity value (80mm/hr) for MAG-1 is observed between hour 24 and hour 26 when the cyclone intensified from a category 2 to a category 3 cyclone, at about 60km away from MAG-1's pixel.

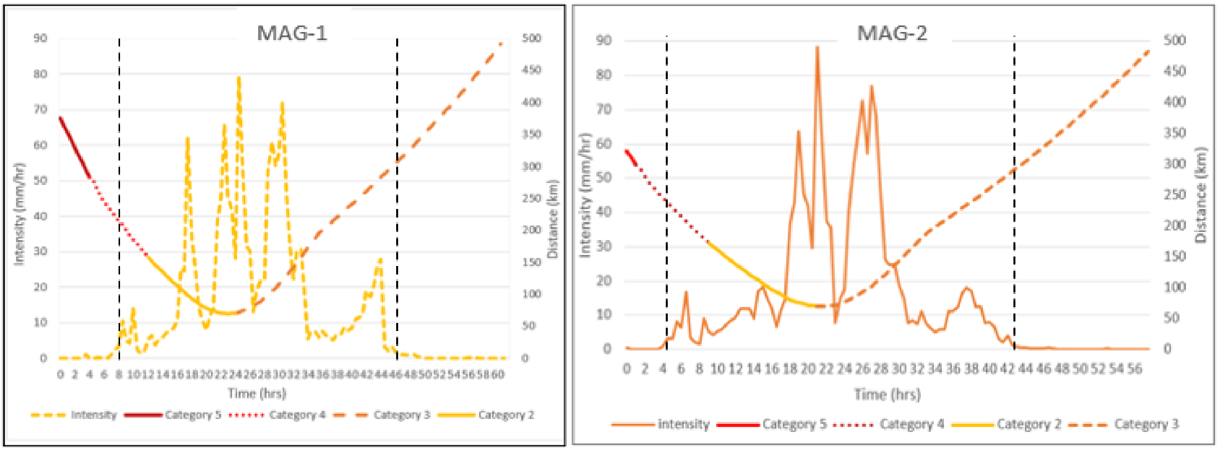

Figure 5.3: Time series plots against the corresponding distance and TC category at each 30minute interval for MAG-1 (left) and MAG-2 (right) plotted from the first till the last non-zero intensity values for each pixel. The vertical fragmented black lines show the beginning and end time step simulated in LISEM.

MAG-2 (Figure 5.3 right) shows a rainfall duration of 56 hours, four hours shorter than the 60 hour duration for MAG-1. The first non-zero rainfall intensity for MAG-2 was recorded when the centre of TC Maria's eye was roughly 350km away, with the last rainfall intensity being recorded when the cyclone's eye was approximately 490km from the centre of MAG-2's pixel. Similar to MAG-1, rainfall intensity values >2mm/hr are observed when TC Maria's eye centre is less than 300km from the pixels centre. Unlike MAG-1 (Figure 5.3, left) with five major intensity peaks (over 40mm/hr), MAG-2 (Figure 5.3, right) shows four peak intensities. The four peaks of MAG-2 occurred when the TC's eye was between 50-100km away from the centre of MAG-2's pixel. The peaks are observed between hour 16, when the TC is a category 2 cyclone until hour 32, when the TC is a category 3. The highest peak intensity value is observed during hour 22 when the cyclone's eye is about 65km away from MAG-2's pixel. Similar to MAG-1, the highest peak intensity value (88mm/hr) for MAG-2 was observed as TC Maria intensified from a category 2 to a category 3 cyclone.

5.2 Rainfall intensity

Next to rainfall magnitude, maximum rainfall intensities produced by TC Maria were analysed (section 3.2.2). Figure 5.4 shows the result of the maximum intensity values within TC Maria's 500km eye radius, obtained from each of the 769 pre-processed GPM IMERG final run precipitation files, described in section 3.1. On average, TC Maria produced maximum intensity values between 20mm/hr and 80mm/hr throughout its lifetime. Highest maximum intensities from TC Maria show values of over 100mm/hr observed in four sections, (i) when the TC was intensifying from a category 2 to a category 3 cyclone at image 229, (ii) as a category 3 cyclone at image 241, (iii) as a category 3 cyclone at image 300, and (iv) as a tropical storm at image 622. Generally, the maximum intensity values as recorded in each pre-processed GPM IMERG precipitation file, seem to follow a wave pattern. The observed maximum intensity values per GPM precipitation file alternate between high and low values, disregarding the category of the cyclone. Maximum intensity values observed when the eye of TC Maria was over Dominica (left side black oval in Figure 5.4) and Puerto Rico (right side black oval in Figure 5.4) range between 30mm/hr to 70mm/hr, which falls within the average maximum intensity range. The maximum intensity values observed before, during and after the TC made landfall on both Dominica and Puerto Rico islands, fall in line with the observed average values throughout TC Maria's observation period, as given by the IBTrACS database. Simply put, the recorded maximum intensity values from TC Maria show no visible differences between the time the TC's eye was over land or water.

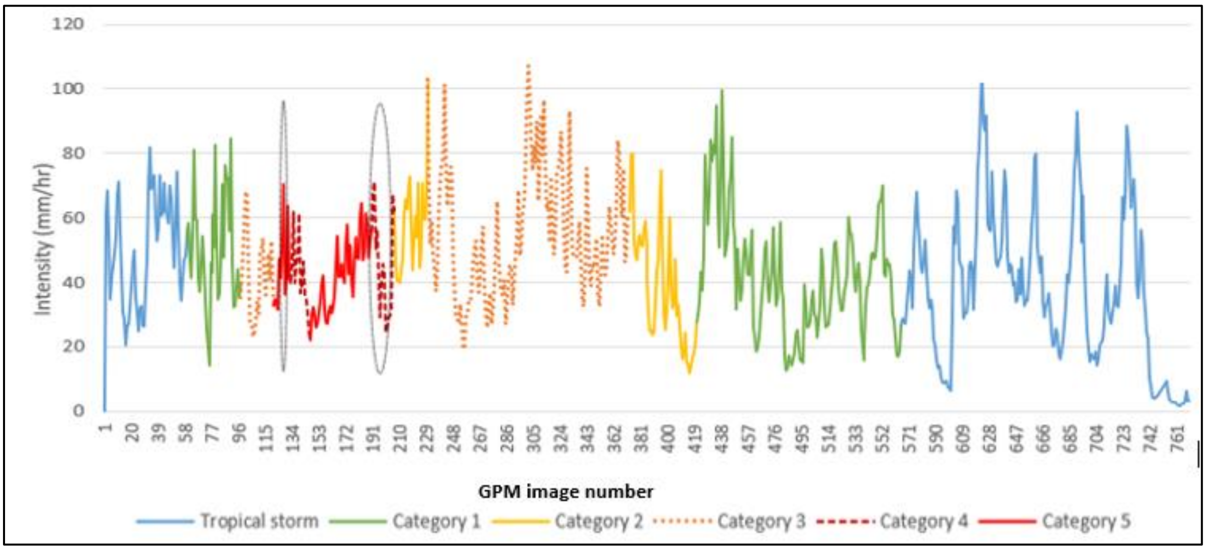

Figure 5.4: Time series of maximum intensity values (mm/hr) observed from the 16th of September 2017 (12:00:00) to the 3rd of October 2017 (11:59:59). The black oval shapes show the maximum intensity values in each precipitation image at the time the eye of the TC was over Dominica (left) (19 September 00:30 – 02:30 UTM), and Puerto Rico (right) (20 September 10:00 – 16:00 UTM). Colour coding shows the TC category at the time of observation.

Figure 5.4 gives an indication of the maximum intensities observed per GPM IMERG file but not the actual number of pixels over the threshold value, as a single image can contain more than one pixel with an intensity value equal to the maximum of the image. Taking a threshold value of 100mm/hr in defining highest intensity values resulted in eight pixels. Of the resulting eight pixels; one pixel from image 229 gave an intensity value of 103mm/hr; one pixel from image 241 had an intensity value of 101.5mm/hr; three pixels from image 300 showed intensity values of 107mm/hr; and three pixels from image 622 to image 625 recorded intensity values between 100mm/hr and 101.8mm/hr. To reduce the number of pixels to analyse, as a proof of concept, the threshold value was increased to 102mm/hr which resulted in four pixels. Figure 5.5 shows the spatial distribution of the four pixels with intensity values > 102mm/hr. The three pixels with the same intensity values (107mm/hr) shown by the orange triangle, green circle, and red cross, show small spatial variations as compared to the pixel with an intensity value of 103mm/hr shown by the black pentagon. The three pixels with the intensity value of 107mm/hr are observed when TC Maria is a category 3 cyclone whereas the pixel (depicted by the black pentagon) with an intensity value of 103mm/hr is observed shortly after TC Maria intensified from a category 2 to a category 3 cyclone.

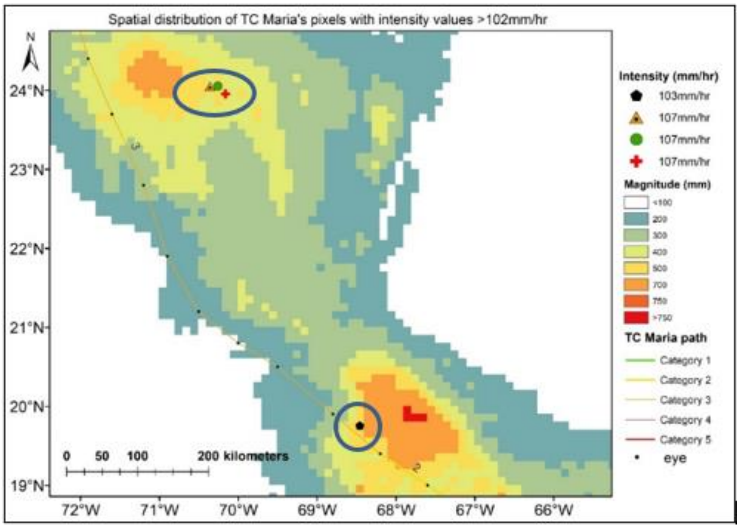

Figure 5.5: Spatial distribution of the pixels with intensity values > 102mm/hr observed from the passing of TC Maria from the 16th of September 2017 to the 3rd of October 2017. The oval inserts provide visual aid in identifying the pixels.

5.2.1 Time series analysis of the highest intensity pixels

Time series plots of the highest intensity pixels were necessary to select high intensity rainfall scenarios for flood modelling. Figure 5.6 shows the time series result of the pixels depicted in Figure 5.5. Colour coding used in Figure 5.5 to show the spatial distribution of the pixels is coordinated to the time series plots in Figure 5.6. The three pixels (orange triangle, green circle and red cross in Figure 5.5) with equal intensity values (107mm/hr), show similar time series structures, depicted by the fragmented orange line, solid green line and the red dotted line in Figure 5.6. A difference in the structure and timing of the time series plots is seen for the pixel with an intensity value of 103mm/hr (solid black line in Figure 5.6).

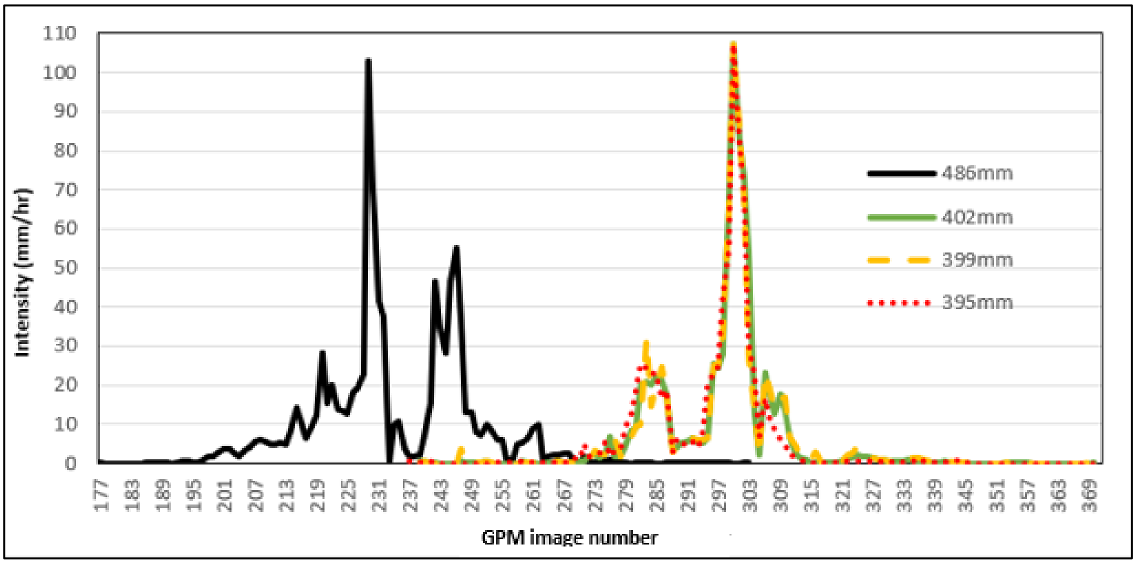

Figure 5.6: Rainfall time series and magnitude values for pixels with intensity values higher than 102mm/hr, plotted against the precipitation image number from the first to the last non-zero intensities observed.

Similar to the highest magnitude pixels, discussed in 5.1.1, two scenarios were chosen from the highest intensity pixels. These scenarios referred to, from here on after, as INT-1 and INT-2, depict the pixel with the highest overall intensity (solid green line in Figure 5.6), and the pixel with the highest magnitude amongst the highest intensity pixels (solid black line in Figure 5.6) respectively, with magnitude value being considered on the overall intensity scenario.

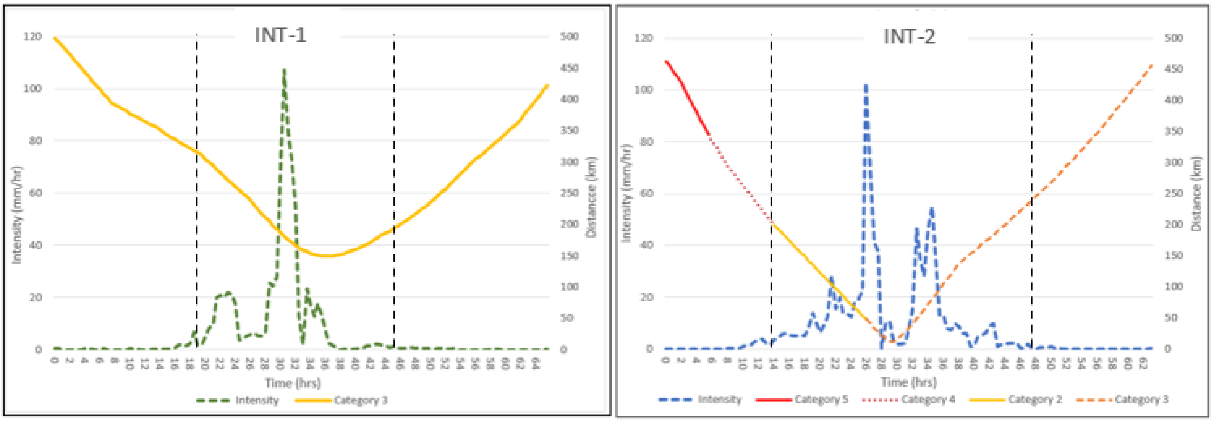

Figure 5.7: Time series plots for INT-1 (left) and INT-2 (right) showing the distances from the centre of the TC's eye to the centre of the observed pixel as well as the TC category at each plot of the time series. The vertical fragmented black lines show the beginning and end time step simulated in LISEM.

In addition to the differences between INT-1 and INT-2's magnitude and intensity values, the two intensity scenarios show distinct differences in terms of number of peaks, duration of the cyclone and the position of the tropical cyclone's eye in relation to the centre of each pixel when an intensity value is recorded. Figure 5.7 shows the time series plots of INT-1 (left) and INT-2 (right) against the distances of the pixel centres to the location of TC Maria's eye at each observation. The first non-zero rainfall intensity value for INT-1 is observed when the eye of the TC is roughly 500km away from INT-1's pixel, and the last intensity value is observed 66hours later, when the TC's eye is approximately 440km away from the pixel. For INT-2, the first non-zero intensity values are observed when the TC's eye is about 450km away from the pixel's centre, and the last intensity value is observed 62hours later, when the TC's eye is roughly 450km away from INT-2's pixel. All measured rainfall intensity values in INT-1 resulted from a category 3 cyclone, with the highest intensity value being recorded around hour 30, when the TC was at a distance of 200km from the centre of INT-1's pixel. Contrasting to INT-1 which has only one peak value, INT-2 shows three peaks. The first peak in INT-2, which is also the highest of the two peaks, occurs at hour 26, when the TC's eye is roughly 10km away from the pixels' centre, and as the cyclone intensified from category 2 to category 3. INT-2's second peak value is observed between hour 34 and 36, when the TC is a category 3 cyclone approximately 100km away from the centre of INT-2's pixel. Despite the occurrence of rainfall on INT-1 and INT-2's pixel when the centre of TC Maria is over 400km away, intensity values >2mm/hr are only observed when the centre of TC Maria's eye is less than 350km away from INT-1 and less than 250km from INT-2's pixel.

5.3 Comparative summary of rainfall scenarios

A cumulative rainfall plot (section 3.3) was made to compare the rainfall characteristics of the selected TC scenarios (MAG-1, MAG-2, INT-1, INT-2) and the selected design storm scenario. Figure 5.8 shows the resulting cumulative rainfall plots of the five rainfall scenarios. Overall, the 100-year design storm shows a rather different rainfall structure as compared to the TC scenarios. The design storm shows an extremely steep slope as a result of the absence of dry spells on the shape of the design storm (Figure 2.5). The four TC scenarios, on the other hand, show high resemblance in rainfall structure with MAG-1 and MAG-2 being more related as are INT-1 and INT-2. Unlike the 100-year design storm scenario which shows a uniform gradient, the TC scenarios show varying gradients along the cumulative plot as an indication of several peaks. Of the five rainfall scenarios, the 100-year design storm shows the earliest cumulative rainfall totals followed by MAG-2 and MAG-1. The high intensity scenarios, INT-1 and INT-2 show the latest cumulative rainfall values with INT-1 showing the latest rainfall cumulative values of all scenarios.

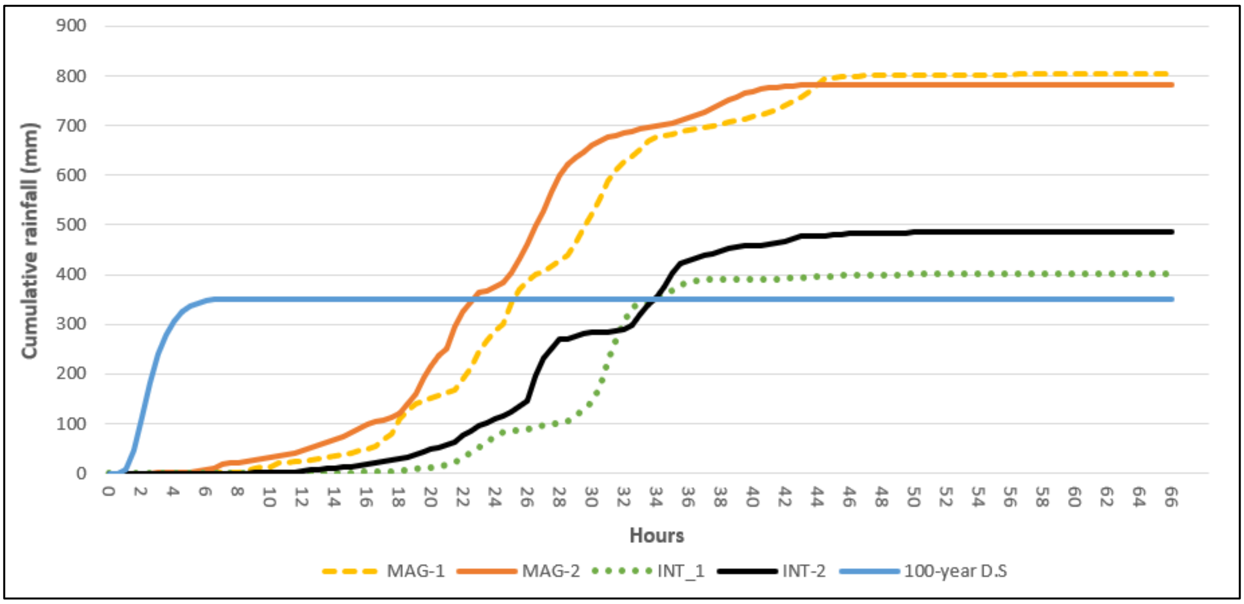

Figure 5.8: Cumulative rainfall plot for the four TC pixels and the 100-year design storm.

Following the detailed rainfall characteristics provided in the sections above, Table 1 summarises the differences in rainfall characteristics for the five rainfall scenarios.

Table 1: Summary of the rainfall characteristics of the TC pixels and the 100-year design storm.

	MAG-1	MAG-2	INT-1	INT-2	100-year DS
Magnitude (mm)	803	783	402	486	350
Magnitude (mm) (rainfall >2mm/hr)	798	778	387	472	349
Duration (hrs) (rainfall >0mm)	60	56	66	62	6.6
Duration (hrs) (rainfall >2mm/hr)	39.5	38	36.5	32	6.1
Maximum Intensity (mm/hr)	80	88	107	103	143
Number of peaks (>40mm/hr)	5	4	1	3	1
Time to the highest peak (hrs)	25	22	30	26	2
Cyclone category at highest peak	2 to 3	2 to 3	3	2 to 3	-
TC eye distance for first intensity (km)	400	350	495	450	-
TC eye distance for last intensity (km)	495	490	440	450	-
TC eye distance for intensity >2mm/hr	300	300	350	250	-
TC eye distance at maximum intensity (km)	60	65	160	50	-
Shortest distance from the eye (km)	60	65	150	10	-

CHAPTER 6 FLOOD MODELLING RESULTS

The results presented in this chapter were obtained after simulating the selected TC scenarios and the 100-year design storm (Chapter 4). The results of the simulation are explained first by qualitative comparisons through visual inspection for the flood start times, flood depth and extent maps. Thereafter, a quantitative description of the flood height and flood extent will be given by looking at the flood extent per flood height class (section 6.3) and the flood volume per flood depth class (section 6.4).

6.1 Flood start time

The results of the flood start time for the Roseau catchment are presented in Figure 6.1. The 100-year design storm shows all pixels to be flooded within the first four hours of the simulation. The TC scenarios show a delayed flood start time with a number of pixels shown to be flooded over 12 hours after the start of the simulation. The observed flood start times correspond with the rainfall structures shown by the cumulative plot of Figure 5.8. Through visual inspection, MAG-2 shows higher number of pixels with a flood start time between 0 and 2 hours, followed by MAG-1, INT-2 and INT-1.

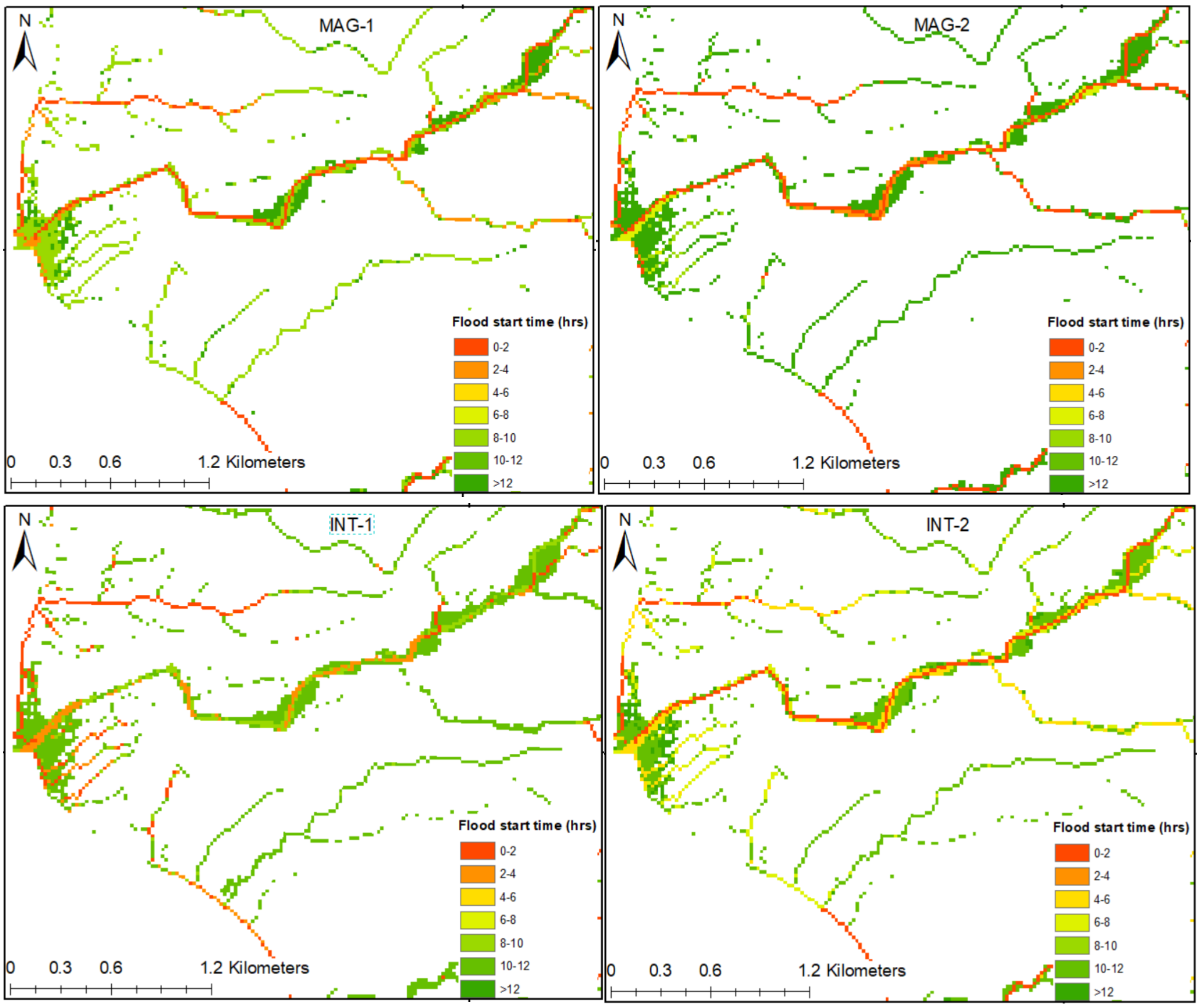

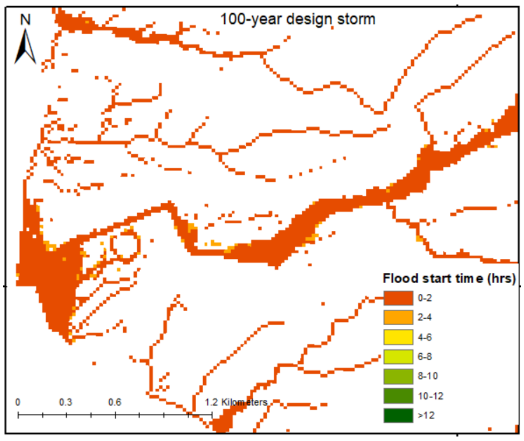

Figure 6.1: Flood start time for Roseau catchment computed from the five rainfall scenarios.

The results of the flood start times for the Grand Bay catchment are shown in Figure 6.2. Similar to Roseau catchment, the flood start times observed in Grand Bay catchment correspond with the cumulative rainfall plot in Figure 5.8. Although the order by which the scenarios show flood start time in Grand Bay is the same as in Roseau catchment, Grand Bay catchment shows higher number of pixels with much later flood start times than that shown in Roseau catchment. The later flood start times for Grand Bay catchment can be explained by the higher infiltrations in Grand Bay catchment shown by the infiltration maps attached as Appendix 5..

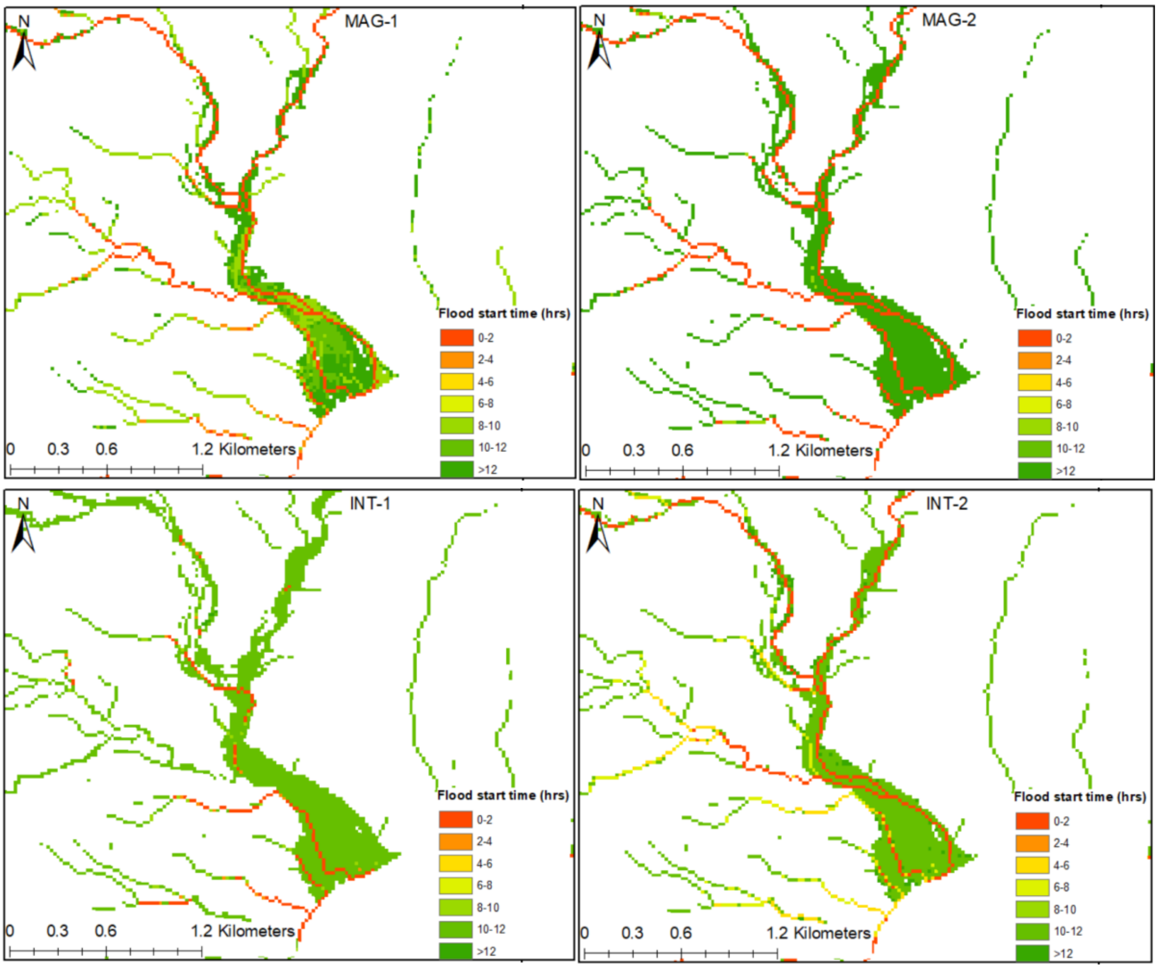

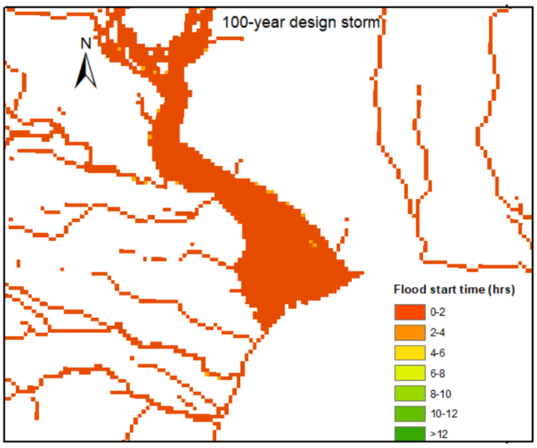

Figure 6.2: Flood start time for Grand Bay catchment simulated from the five rainfall scenarios.

6.2 Flood height

Maximum flood height maps for Roseau and Grand Bay catchments from the five rainfall scenarios are shown in Figure 6.3 and Figure 6.4, respectively. Visual inspection of the catchments shows similar patterns in the catchments flood extent more evidenced in the four TC scenarios. The water runoff seems to flow along the terrain of the island (Figure 2.2) into the watershed channels where the flood then expands from the filling of the river channels.

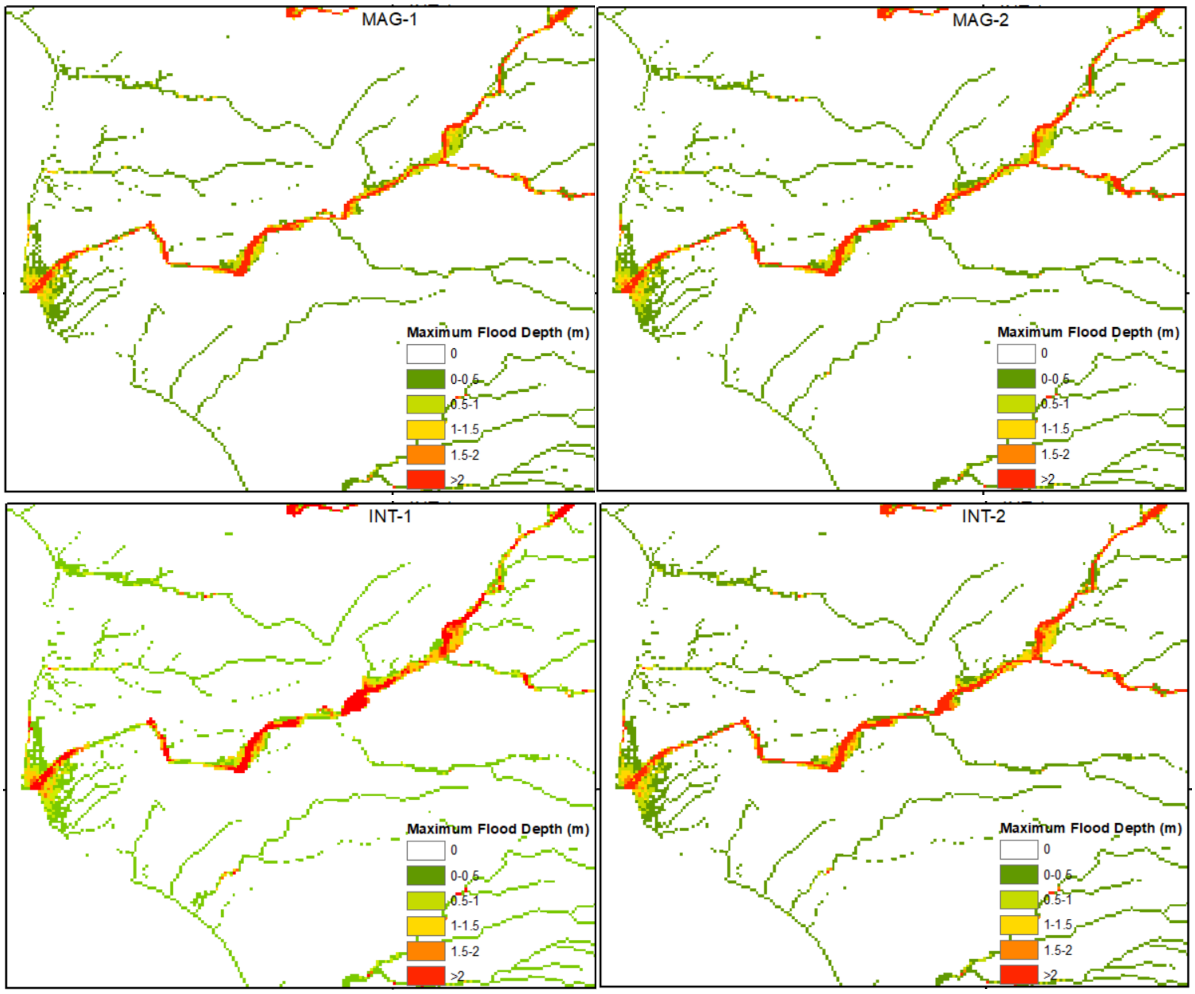

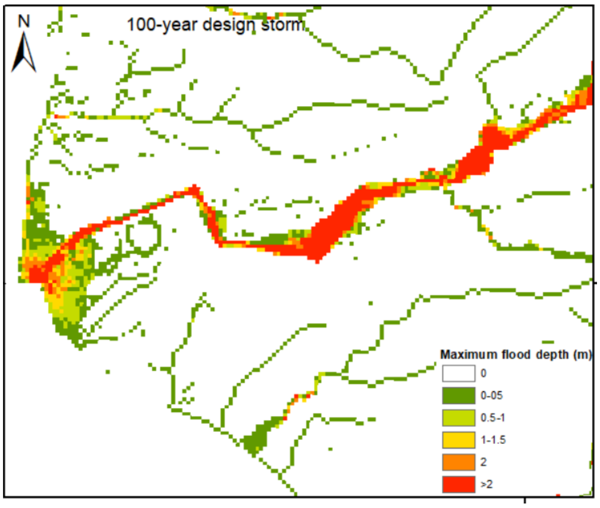

Figure 6.3: Maximum flood height maps for Roseau catchment as simulated by the five rainfall scenarios.

While flood extent shows similar flood patterns for all five scenarios, differences can be observed in the maximum flood height. For both the Roseau and Grand Bay catchments, the 100-year design storm shows a larger area with a flood height >2meters as compared to the TC scenarios. For the TC scenarios, MAG-1 and MAG-2 show generally lower number of pixels with a flood height >2meters compared to the high intensity scenarios, INT-1 and INT-2.

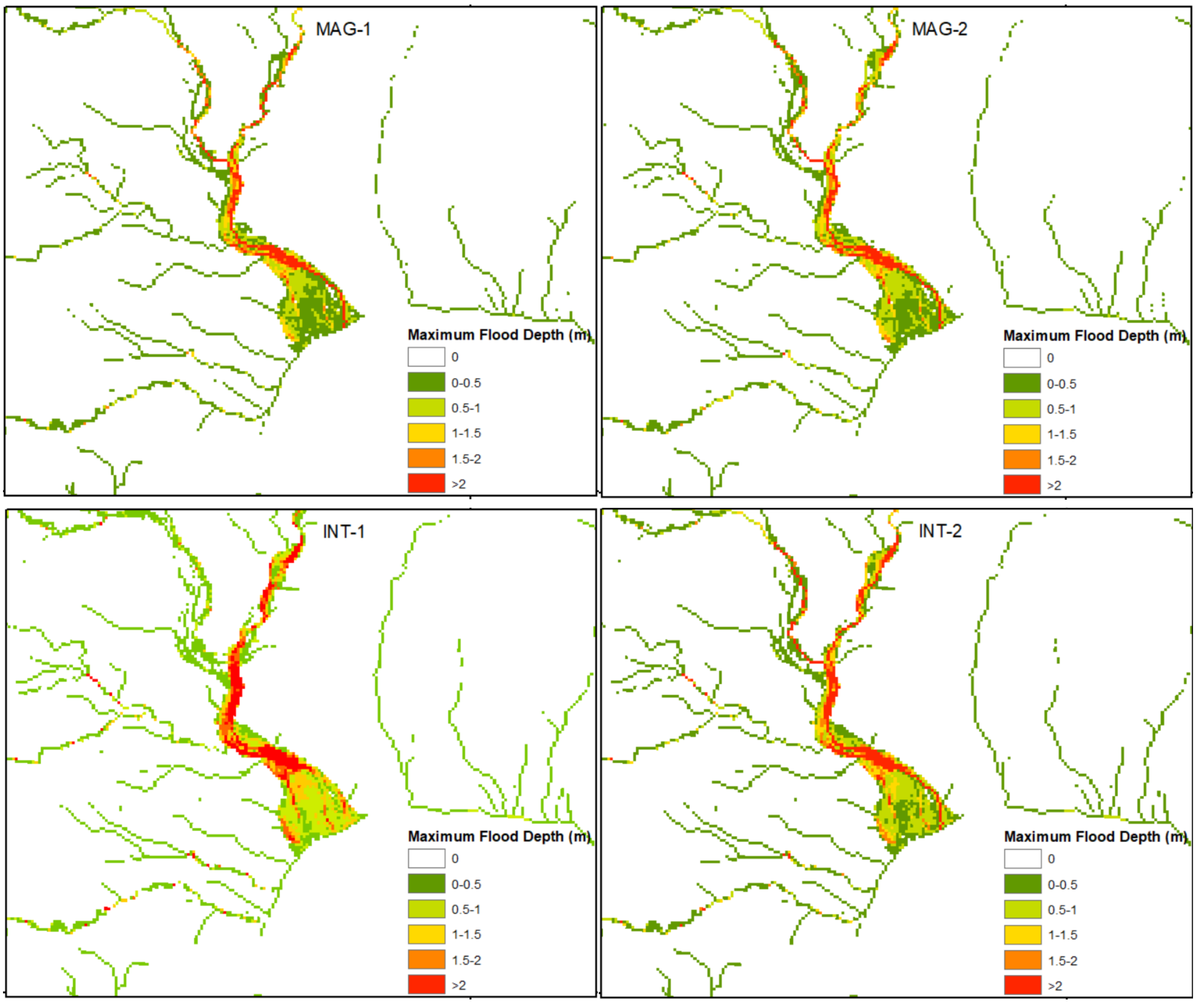

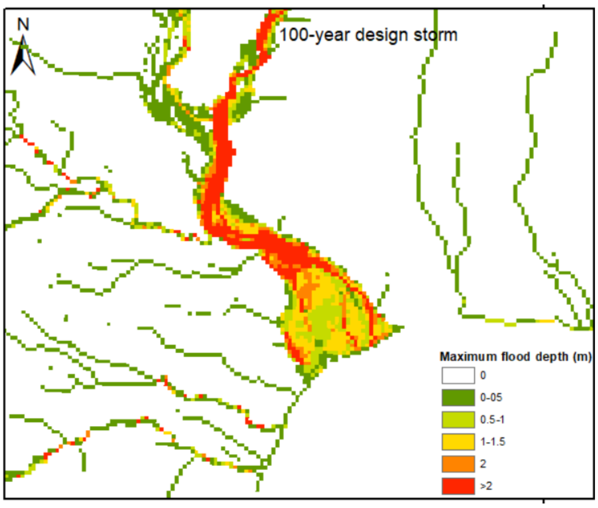

Figure 6.4: Maximum flood height map for Grand Bay catchment.

6.3 Flood extent

Sections 6.1 and 6.2 provided a generalised comparison of the flood characteristics from the five rainfall scenarios. To allow for a more detailed comparison, a quantification was done for the flood extent per flood height class as described in section 4.6.4. Figure 6.5 and Figure 6.6 shows the resulting flood extent for Roseau and Grand Bay catchments, respectively, computed from the five rainfall scenarios. The overall flood extent, per scenario, plotted against the simulated magnitude and maximum intensity is shown on the top graph of Figure 6.5 (for Roseau) and Figure 6.6 (for Grand Bay). The bottom graphs of Figure 6.5 and Figure 6.6 give more details of the flood extent by showing the percentage area flooded within each flood height class.

For Roseau catchment, the total flood extent seems to be influenced by the maximum intensity of a scenario. Higher intensity scenarios show a higher overall flood extent as compared to lower intensity scenarios (top graph of Figure 6.5). When looking at the percentage flood extent per flood height class (bottom graph of Figure 6.5), the TC scenarios show highest flood area percentages for flood height classes <2meters. The 100-year design storm, on the other hand, shows a higher percentage (30%) of its flooded extent to result from a flood height class >5meters. Though slightly less than INT-1 on the overall flood extent, INT-2 shows, amongst the TC scenarios, the highest flood percentage (10%) for flood height >5meters.

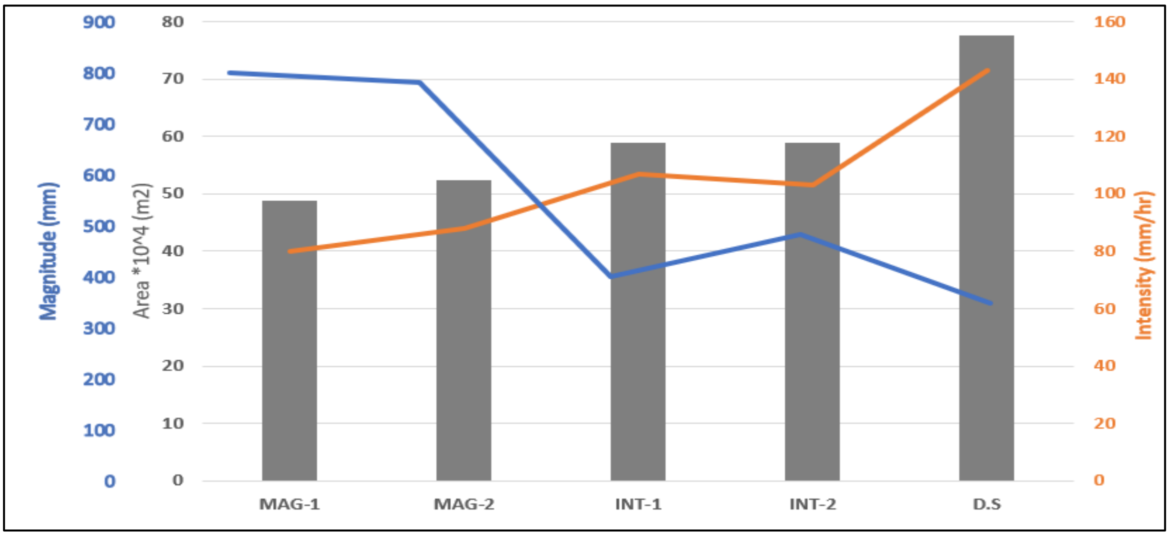

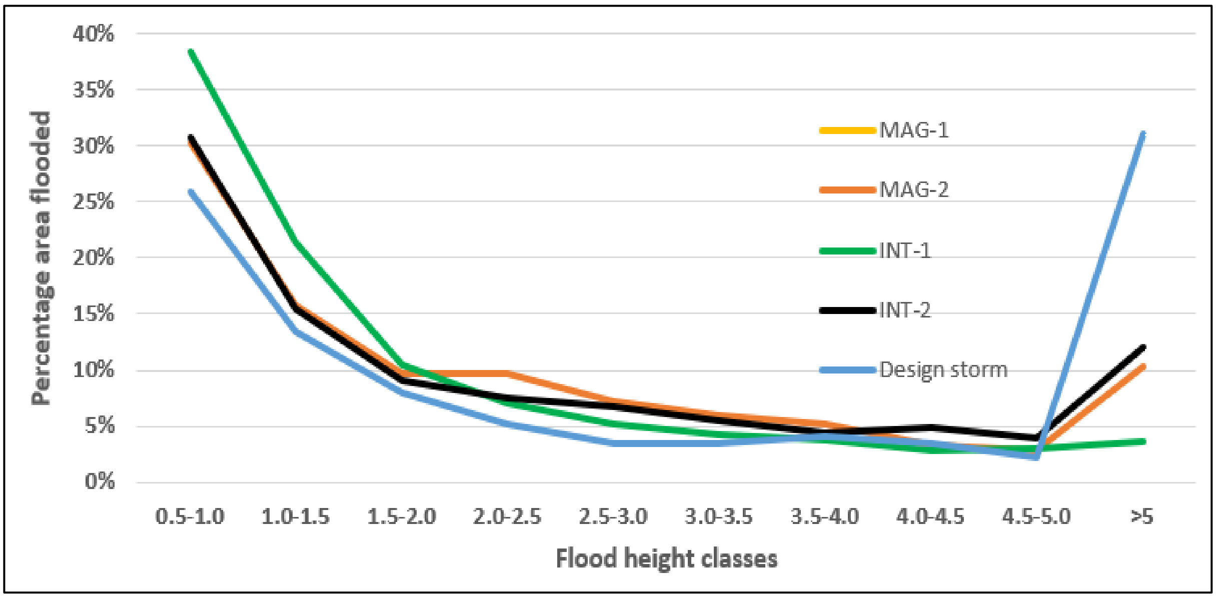

Figure 6.5: Quantitative comparison of Roseau's flood extent for the five rainfall scenarios. The overall flood extent per scenario, shown on the top graph is plotted against the simulated magnitude (blue plotted line; left Y-axis) and the maximum intensity (orange plotted line; right Y-axis). The bottom graph shows the percentage area flooded per flood height class for the five rainfall scenarios.

Similar to the flood extent shown on Roseau catchment, the Grand Bay catchment shows higher flood extents to result from higher intensity scenarios. The reason for the lesser flood extent from high magnitude scenarios can be explained by the higher infiltration totals (Appendix 5) and the large total volume outflow (Table 2) in high magnitude scenarios as compared to high intensity scenarios. The 100-year design storm shows the highest overall flood extent with over 30% of the flood extent to be from flood height >5meters. For the TC scenarios, INT-1 shows the highest overall flood extent but has the least flooded area (<2%) of all rainfall scenarios for flood height>5meters. INT-2 on the other hand shows the highest flood area percentage of 5% for flood height >5meters.

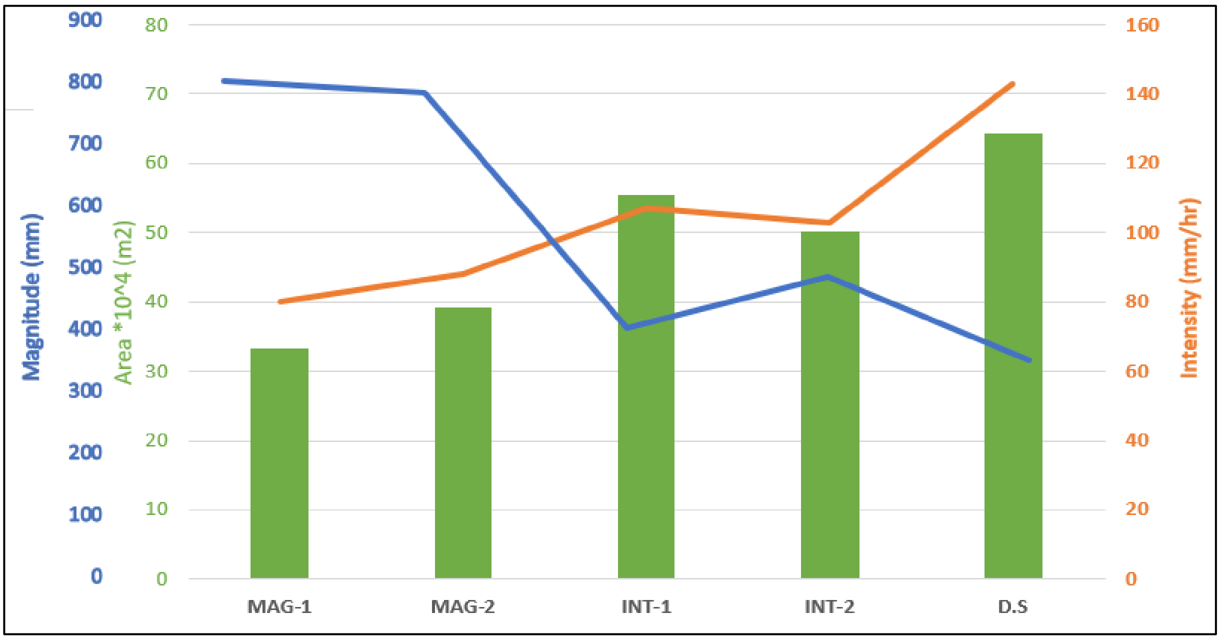

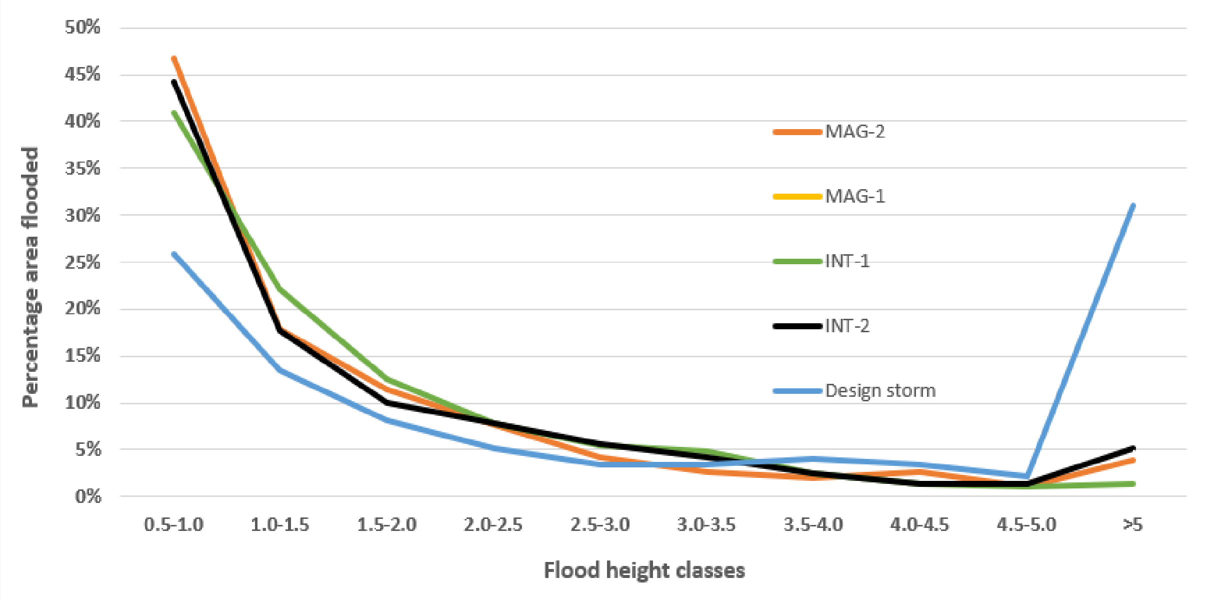

Figure 6.6: Quantitative comparison of Grand Bay's flood extent for the five rainfall scenarios. The overall flood extent per scenario, shown on the top graph is plotted against the simulated magnitude (blue plotted line; left Y-axis) and the maximum intensity (orange plotted line; right Y-axis). The bottom graph shows the percentage area flooded per flood height class for the five rainfall scenarios.

6.4 Flood volume

Similar to the flood extent, quantitative comparisons were done for the flood volume per flood height class as described in section 4.6.3. Figure 6.7 and Figure 6.8 show the resulting flood volume for Roseau and Grand Bay catchments, respectively, computed from the five rainfall scenarios. The overall flood volume per scenario plotted against the simulated magnitude and maximum intensity is shown on the top graphs of Figure 6.7 (for Roseau) and Figure 6.8 (for Grand Bay). The bottom graphs of Figure 6.7 and Figure 6.8 give more details of the flood volume by showing the flood volume percentage within each flood height class for Roseau and Grand Bay catchments, respectively.

Starting with the Roseau catchment (Figure 6.7), the 100-year design storm shows the highest overall flood volume with approximately 50% of its total flood volume resulting from a flood height class >5 meters (Figure 6.7 bottom). Amongst the TC scenarios, INT-2 shows the highest overall flood volume followed by MAG-2. INT-1 and MAG-1 show the least flood with approximately equal flood volumes. The flood volume percentages show INT-1 to have its highest flood volume percentage in the lower flood height class (0.5-1.5) and the least flood volume percentage of all scenarios from a flood height class >5meters. MAG-1, MAG-2 and INT-2 show low flood volume percentages for flood height classes <5meters but much higher flood volume percentage for flood height class >5 meters as compared to INT-1.

Considering the scenarios' simulated magnitude (blue plot in Figure 6.7 top) and maximum intensity values (yellow plot in Figure 6.7 top) shows a positive relationship between the flood volume and the maximum intensity. Higher maximum intensities show higher flood volumes for all scenarios except for INT-1 where catchment properties and the rainfall structure could have influenced the total flood volume. High rainfall magnitudes show to have overall lower flood volumes owing to the high outflow volumes and high infiltration values shown in Table 2 and Appendix 5. MAG-1 for instance, has the highest magnitude of all five scenarios but gives the least flood volume. Seemingly, the 100-year design storm has the least magnitude of all five scenarios but gives the highest overall flood volume. The high intensity scenarios, INT-1 and INT-2, have almost half the magnitude of MAG-1 and MAG-2 but show rather similar flood volumes with INT-2 showing a much higher flood volume than the high magnitude scenarios. The insignificant influence of the rainfall magnitude can be explained by the higher outflows in high magnitude scenarios as compared to lower magnitudes (Table 2) as well as the higher infiltration rates associated with lower rainfall intensities (Appendix 5).

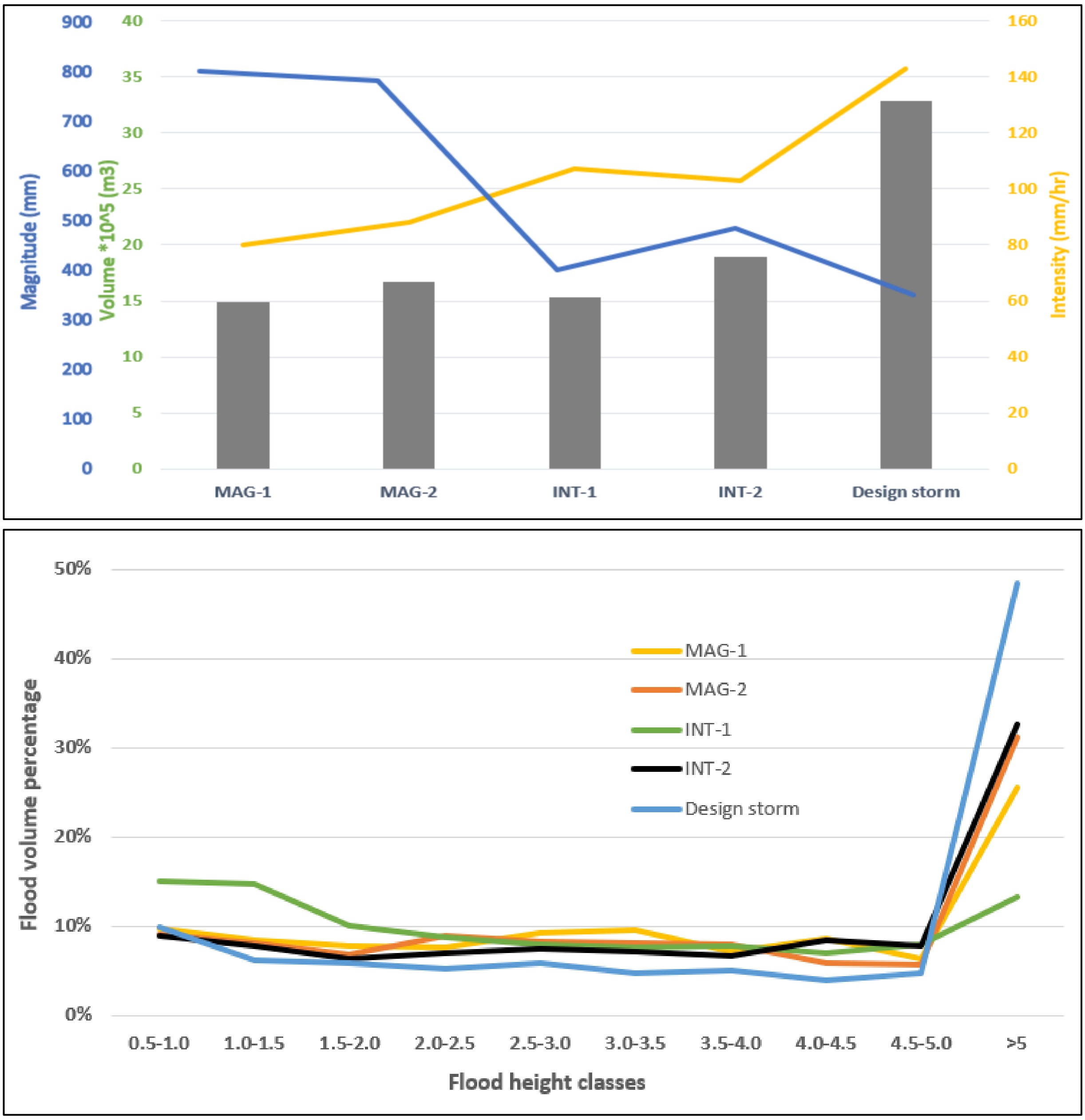

Figure 6.7: Quantitative comparison of Roseau's flood volume for each of the five scenarios. The overall flood volume per scenario plotted against the simulated magnitude (blue plotted line; left Y – axis) and the maximum intensity (yellow plotted line; right Y-axis) is shown on the top graph. The bottom graph shows the percentage volume per flood height class for the five scenarios.

Similar to Roseau catchment, rainfall intensity values show to have huge influences on Grand Bay's flood volume for all five scenarios. The overall highest flood volume is observed in the design storm scenario, followed by INT-1 and INT-2 with equal flood volumes. MAG-1 with the least rainfall intensity of all five scenarios shows the least overall flood volume.

The percentage of flood volume per flood height class given in the bottom graph of Figure 6.8 shows the 100-year design storm to have roughly 28% of its total flood volume resulting from flood water height >5meters. Although INT-1 shows a highest overall flood volume in comparison to the TC scenarios, the scenario shows higher flood volume percentages to result from flood height classes < 4meters. Only 5% of the total flood volume in INT-1 results from a flood height class >5meters. The other three TC scenarios (MAG-1, MAG-2 and INT-2) showed higher flood volume percentages for flood height >5meters as compared to INT-1 with INT-2 showing the highest percentage (20%) of the flood volume to result from a flood height class >5meters.

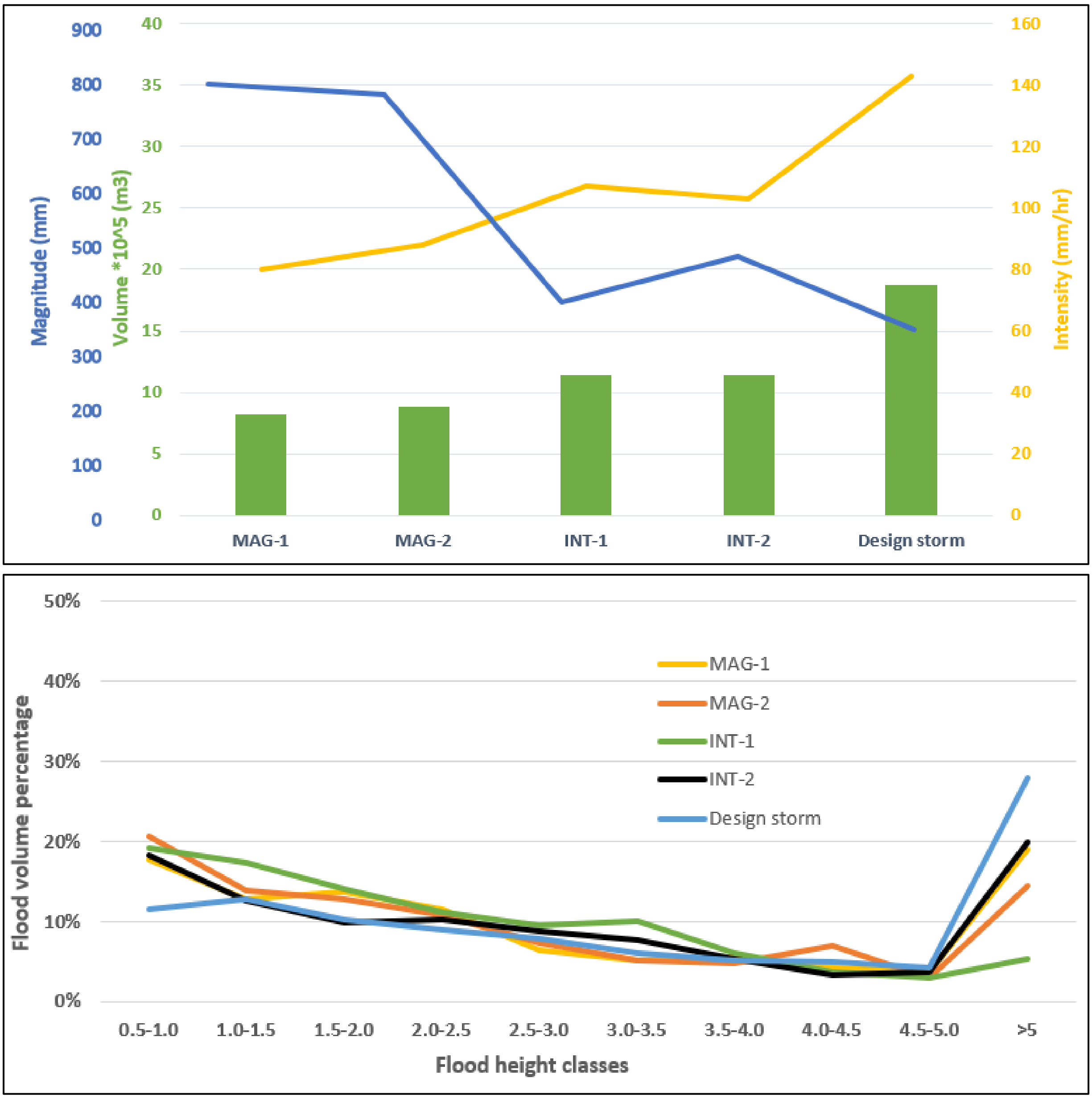

Figure 6.8: Quantitative comparison of Grand Bay's flood volume for the 5 rainfall scenarios. The overall flood volume per scenario plotted against the simulated magnitude (blue plotted line; left Y–axis) and the maximum intensity (yellow plotted line; right Y-axis) is shown on the top graph. The bottom graph shows the percentage volume per flood height class for all rainfall scenarios.

6.5 Comparative summary of the flood characteristics

Table 2 is used to summarise the resultant flood characteristics and the catchment responses that influenced the resulting flood characteristics. Overall, the high intensity scenarios, INT-1 and INT-2 simulated the largest flood extent, highest flood height and the highest flood volumes in comparison to the high magnitude scenarios, MAG-1 and MAG-2. Of the high intensity scenarios, INT-2 shows overall higher flood characteristics as compared to INT-1, making INT-2 the worst-case rainfall scenario of the TC scenarios.

Table 2: Quantitative summary of the flood modelling results.

	MAG-1	MAG-2	INT-1	INT-2	100yr-Design Storm
Simulated Magnitude (mm)	755	746	387	470	350
Maximum Intensity (mm/hr)	80	88	107	103	145
Total infiltrated volume (mm)	299	288	145	190	94
Total outflow (mm)	452	454	238	276	294
Roseau flood extent (m^2) >0.05m	48.84	52.31	58.92	58.96	77.56
Total volume Roseau (m^3) $*10^5$	14.87	16.67	15.36	18.98	32.87
Discharge for Roseau (m^3) $*10^5$	3.17	3.20	3.22	3.44	5.51
Grand Bay flood extent (m^2) >0.05m	33.36	39.16	55.40	50.24	64.32
Total volume for Grand Bay (m^3) $*10^5$	8.24	8.89	11.43	11.43	18.73
Discharge for Grand Bay (mm) $*10^5$	3.24	3.54	4.73	4.07	5.95

6.6 Implications of the simulated flood results

The 100-year design storm shows shorter flood start times, larger flood areas and higher flood volumes with flood heights > 5meters. Taking INT-2 as the worst-case rainfall scenario from a TC event would imply an overestimate of the flood characteristics simulated by the 100-year design storm. The relatively short flood start times modelled by the 100-year design storm imply the incapability of the design storm to be used in early warning and evacuation planning. Although the simulated flood extent shows minor differences between the 100-year design storm and INT-2 suggesting that flood areas are mapped well in both cases, the 100-year design storm showed higher percentages of flood extent to be from flood height classes >5meters. Economically, the high flood heights simulated by the 100-year design storm suggests the need for high infrastructures when establishing flood mitigation measures. Given Dominica's low GDP (Adom, 2018; Aon Benfield Analytics, 2018), overestimated mitigation measures poses a financial burden on the Island. Dominica will have to plan and establish high mitigation measures which will be more costly in construction and maintenance.

CHAPTER 7 DISCUSSION AND CONCLUSION

The main aim of this research was to develop a worst-case TC rainfall scenario and evaluate the flood implications from simulating the worst-case TC rainfall scenario against a design storm of comparable rainfall characteristics. In the first objective, a method was developed to extract and analyse extreme rainfall pixels from the pathway of TC Maria. For the second objective, a comparison was made between the flood characteristics from the selected TC scenarios against flood characteristics simulated from Dominica's 100-year design storm. For each objective, a discussion is made on the overall findings with a critical assessment made on the robustness of the data and methods used to obtain the presented results.

7.1 First objective

RQ 1.1: What strategy can be used to extract extreme TC rainfall pixels from a TC pathway given temporal layers of satellite precipitation images?

With respect to the first research question (RQ1.1), a method was developed for extracting extreme rainfall pixels from TC Maria's precipitation images. Figure 7.1 shows the flow chart of the steps used to extract the extreme rainfall pixels of TC Maria. When developing the TC rainfall extraction strategy, a number of choices were made. The robustness of the choices made can be reviewed by discussing on each individual choice.

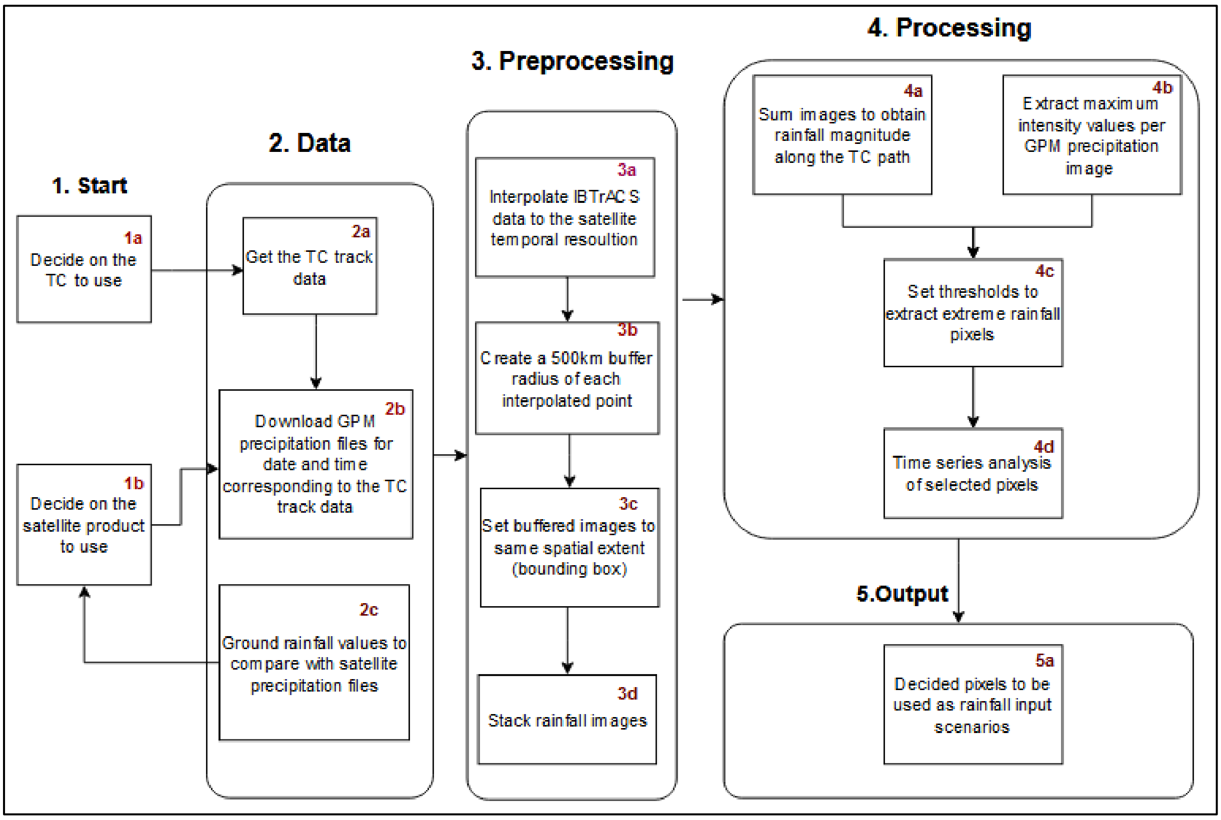

Figure 7.1: Flowchart to select extreme rainfall pixels for analysis. Numbers highlight the order in which the steps were carried out.

Data

First and foremost, a choice was made to use one TC. Given, however, the erratic nature of TCs (Emanuel, 2017; Jiang et al., 2008), the results of one cyclone cannot be generalised for all TCs. Nevertheless, as the research was done to develop a method as a proof of concept, the use of a single TC was sufficient for achieving the research's objective. The use of the 2017 Atlantic Basin TC Maria stands as a justifiable choice as it presented diverse characteristics. The cyclone underwent all five TC categories, made two landfalls, and produced record flooding in Puerto Rico and Dominica islands. The diversity of TC Maria gave the possibility of observing TC rainfall characteristics under diverse conditions.

Regarding the precipitation datasets. The choice to use the GPM IMERG Final run precipitation estimates was based on the satellite's high temporal and spatial resolution in comparison to other satellite precipitation instruments. Although the high resolution offered by the GPM satellite instrument makes the instrument attractive to use, it is worth noting that the GPM instrument has been in use for barely five years. The robustness of the instrument to estimate precipitation values has thus not been fully understood (Khan & Maggioni, 2019). The uncertainty of the GPM instrument presents a limitation to the research as the error of the observed values is not known. In an attempt to evaluate the possible error of the instrument for TC Maria's precipitation (Appendix 1), a comparison was made between the GPM IMERG estimates and the ground rainfall estimates reported in the NOAA synoptic reports. Reflecting back on the decision made to compare the two datasets, not much logic is seen. The ground-based rainfall datasets, although usually considered as better rainfall estimates in comparison to satellites, in high wind and extreme rainfall events, the ground-based stations are subject to multiple errors. The conclusion made is that true rainfall is unknown and remains an estimate. Based on this conclusion, the GPM IMERG Final run precipitation estimates can be accepted as the best available rainfall estimates for use in TC rainfall extraction.

Methods

The choice of the buffer value used to define the extent of TC Maria's rain bands was very important for precise extraction of TC Maria's rainfall. If the rainfall extent is underestimated, essential TC rainfall information is lost. An overestimation of rainfall extent may lead to the incorporation of non TC related rainfall values (Zhou & Matyas, 2018). A 500km buffer radius, adopted from previous studies (F. J. Chen & Fu, 2015; Ramos-Scharrón & Arima, 2019) and used for this research proved to be adequate for extracting TC Maria's rainfall values. The results of the time series plots against the TC distance (sections 5.1.1 and 5.2.1) showed low intensity values (<2mm/hr) when the cyclone was over 350km away from the studied pixel and the last non zero recorded intensities when the cyclone was roughly 450km away. Although the 500km buffer value proved to be sufficient for TC Maria, the sufficiency of the radius is not conclusive of rainfall extents of all cyclones. TC rainfall structures ought to be examined to find the optimal radius value that neither excludes essential TC rainfall information nor incorporates non TC related rainfall values for a TC under study.

The developed R-script (Appendix 2) allowed for automatic computations of TC Maria's rainfall characteristics. One factor worth discussing in the developed script, was the choice made to compute rainfall characteristics with varying pixel durations. Initially a decision had been made to extract extreme rainfall pixels based on 24hour moving windows so as to make a fair comparison with the rainfall duration used in constructing design storms. The disadvantage of using a moving window was the loss of relevant storm information such as the total rainfall magnitude, duration or the spread of peak intensity values. A new approach was hence taken to compute rainfall magnitudes based on the entire duration of the pixel within the 500km radius. This approach is similar to that used by Begueria et al., (2009). The new approach gave the advantages of allowing for full rainfall event analysis. Unlike ground-based rainfall values which are based on daily rainfall totals and rarely compute entire event magnitudes, the method used in this research makes an analysis of the entire storm duration. The used method thus increases the robustness of the rainfall analysis by allowing for total rainfall event analysis.

When selecting extreme TC rainfall pixels to analyse, a rather important decision is the threshold value to use (Begueria et al., 2009). Given the variability of TC rainfall, using low threshold values to analyse extreme rainfall events reduces the risk of loss of vital information pertaining the dynamics of the TC. In this research, the threshold value used for both intensity and magnitude were selected with the goal of having a small sample size. The use of a smaller sample size is justifiable as the rainfall extraction was done as a proof of concept of the suggested strategy.

RQ1.2: What information can be obtained pertaining to the TC rainfall distribution from using the implimented strategy?

One interesting finding when analysing TC Maria's rainfall distribution was the absence of a direct relationship between TC rainfall and the category of the cyclone (Chapter 6). The results of the research showed the highest magnitude and intensity pixels to have resulted from a category 2 and category 3 cyclone. The finding that highest rainfall volumes could be generated by lower TC categories discredits common conceptions that TCs with higher maximum sustained wind speed (category 4 and 5) produce higher rainfall in comparison to lower category cyclones. This conception is mostly evidenced when issuing out early warnings where the level of warning is related to the category of the cyclone (Meteorological Department Curacao, 2017; Roy, Sarkar, Åberg, & Kovordanyi, 2015). Although the obtained results were based on the analysis of a single TC, which cannot be conclusive for all TCs, our findings confirm with those of Agustín Breña-Naranjo et al., (2015) who proved low correlation of TC rainfall with the TC maximum sustained wind speed. Based on the presence of similar research results, a conclusion can be made on the possibility of lower category cyclones to produce precipitation maxima.

When looking at the location of the selected extreme rainfall pixels (Figure 5.1 and Figure 5.5), high rainfall magnitude and intensity pixels were observed to occur over the Caribbean Sea as compared to inland. This was rather an unexpected finding as some studies have posed the theory of higher rainfall magnitudes and intensities being observed inland due to the presence of frictional surfaces reducing the cyclone's speed (Jiang et al., 2008; Kirshbaum & Smith, 2009; Nugent & Rios-Berrios, 2018). Although preliminary, the contracting findings presented in this research could simply be a proof of spatial variability in TC rainfall. S. S. Chen et al. (2006), shows how TC rainfall is influenced by the presence variations in both environmental and TC factors leading to inconsistencies in high rainfall distributions. Another possible explanation maybe that the GPM IMERG final run gave underestimated rainfall values over land as suggested by the comparisons with NOAA ground based estimates (Appendix 1). An assessment, however, done by Khan & Maggioni (2019), on the accuracy of GPM IMERG in estimating over ocean rainfall showed that overall the GPM IMERG products give underestimates in over ocean rainfall. The study of Khan & Maggioni (2019) suggests possible underestimates in the extreme rainfall pixels observed in this study.

Concerning the overall magnitude distribution of TC Maria (section 5.1), pixels with high rainfall magnitude values were observed to occur in clusters. A probable explanation for the observed clustering could be a longer duration of TC rain band on an area due to the slowing down or turning of the cyclone. This explanation is however speculative as S. Chen et al., (2006), states a number of several other factors that may have influence on TC rainfall distribution. Nevertheless, as TC travel speed has been proved to have an influence on rainfall amounts (Blake & Zelinsky, 2018; Emanuel, 2017) observed clusters are linked to the long duration of a pixel within the 500km radius value.

RQ 1.3 What are the differences in rainfall variability if the worst-case rainfall is to be based on highest magnitude or highest maximum intensity pixels?

The differences in rainfall characteristics (

	MAG-1	MAG-2	INT-1	INT-2	100-year DS
Magnitude (mm)	803	783	402	486	350
Magnitude (mm) (rainfall >2mm/hr)	798	778	387	472	349
Duration (hrs) (rainfall >0mm)	60	56	66	62	6.6
Duration (hrs) (rainfall >2mm/hr)	39.5	38	36.5	32	6.1
Maximum Intensity (mm/hr)	80	88	107	103	143
Number of peaks (>40mm/hr)	5	4	1	3	1
Time to the highest peak (hrs)	25	22	30	26	2
Cyclone category at highest peak	2 to 3	2 to 3	3	2 to 3	-
TC eye distance for first intensity (km)	400	350	495	450	-
TC eye distance for last intensity (km)	495	490	440	450	-
TC eye distance for intensity >2mm/hr	300	300	350	250	-
TC eye distance at maximum intensity (km)	60	65	160	50	-
Shortest distance from the eye (km)	60	65	150	10	-

1) between high magnitude and high intensity pixels were observed through comparing the structures of the time series plots and observing the cumulative plot of each pixel (Chapter 5). Although the cumulative plot proved to be a sufficient tool for explaining the rainfall variability between the high magnitude and high intensity pixels, the stated differences are based on four pixels. The limited number of pixels used marks a limitation as the results cannot be generalised to differences in rainfall variability of other high magnitude and high intensity pixels.

7.2 Second objective

RQ2.1 For Dominica, five design storms were created with return periods of 5, 10, 20, 50 and 100-years with different magnitudes and peak intensities (Jetten, 2016). Which design storm should be used to compare with the TC scenarios?

The 100-year design storm was selected for flood comparisons with the TC scenarios due the design storm's closer rainfall characteristics in comparison to the 5, 10, 20 and 50-year design storms. The adequacy of the 100-design storm to be compared with the TC scenarios can be evaluated by comparing the difference in rainfall characteristics between MAG-1 (Highest overall magnitude, lowest maximum intensity), INT-1 (highest overall intensity, lowest magnitude), and the 100-year design storm. By taking INT-1 as a base for comparison, the differences in rainfall characteristics between the three scenarios are shown in Table 3. Arguing on the large differences in magnitude (401mm) and intensity (27mm/hr) values of the TCs scenarios (MAG-1 and INT-1), the 100-year design storm is concluded to be sufficient for comparison.

Table 3: Difference in rainfall characteristics between MAG-1, INT-1 and the 100-year design storm. INT-1 shows raw magnitude and intensity values whilst MAG-1 and the 100-year design storm show magnitude and intensity values relative to INT-1. The (+) values show higher value than INT-1 and (-) value show lower value than INT-1.

	MAG-1	INT-1	100-year design storm
Magnitude (mm)	**+401**	**402**	**-52**
Intensity (mm/hr)	**-27**	**107**	**+36**

RQ 2.2 How do the flood characteristics of the selected design storm compare with the flood characteristics simulated from the extracted extreme rainfall pixels of the TC?

A somewhat obvious finding to emerge from comparing the flood start times of the simulated scenarios (section 6.1) was the high dependence of the flood start times with the timing of peak intensity values. This finding was expected given the high soil moisture content set to carter for the excluded low rainfall intensity parts of the scenarios. The gradual flood start times observed for TC scenarios highlight the ability of using TC scenarios for early warning and evacuations. The 100-year design storm on the other hand, showed complete flooding within the first four hours of simulation proving incapability of use in early warnings.

Despite the large magnitude and intensity differences between the five rainfall scenarios, minimal differences were observed in the simulated flood extents (section 6.3). The observed similarities in simulated flood extents match the flood extent results presented by Jetten (2016) and Ogden (2016). The similarities observed in simulated flood extents are due to Dominica's steep terrain which buffers the flood effects causing runoff accumulation downstream. Along the coastal areas, where differences in flood extents are more evidenced, larger flood extents were observed in higher intensity scenarios as compared to the high magnitude scenarios. This result collaborates with Dominica's flood hazard maps developed by Jetten (2016) during the CHARIM project. Similar to the results obtained in this research, the results of Jetten (2016) showed higher flood extents to result from Dominica's 5-year design storm which had the highest intensity and lowest magnitude in comparison to the simulated 10, 20 and 50-year design storms.

Regarding the simulated flood volumes, overall, the presented findings showed higher intensity scenarios to give higher flood volumes. Based on this trend, it was expected that the 100-year design storm would produce a higher flood volume, given the scenario's high intensity. However, considering the magnitude of difference between the five scenarios, the large difference of the 100-year design storm suggests an overestimate of the flood volume. Table 4 shows the differences of flood volume between MAG-1 (highest overall magnitude and lowest intensity), INT-1 (Highest intensity and lowest magnitude among the TC scenarios) and the 100-year design storm (Highest overall intensity and overall lowest magnitude). A feasible explanation to the overestimations given by the 100-year design storm is the absence of variations in the design storm's rainfall structure. A study done by Balbastre-Soldevila et al., (2019) showed that different design storm construction methods, though based on the same rainfall dataset, results in different flood characteristics. Based on the findings of this research and that of Balbastre-Soldevila et al., (2019), a conclusion is made that the design storms constructed for Dominica following a probability density shape is not the best shape for the island. The use of the currently developed design storms will simply overestimate the flood characteristics resulting in overestimated mitigation measures.

Table 4: Difference in flood volume between MAG-1, INT-1 and the 100-year design storm. INT-1 shows raw flood volumes whilst MAG-1 and the 100-year design storm show flood volume relative to INT-1. The (+) values show higher value than INT-1 and (-) value show lower value than INT-1.

	MAG-1	**INT-1**	**100-year design storm**
Roseau (m^3) *10^5	-0.4	15.3	+17.6
Grand Bay (m^3) *10^5	-2.9	11.1	+7.6

Concerning the flood characteristics simulated from the TC scenarios, it is interesting to note that despite the differences in rainfall characteristics (magnitude, intensity, number of peaks, etc.), all four TC scenarios showed rather similar flood characteristics (Table 2). The similarities in flood characterises were more pronounced for scenarios within each rainfall group (high magnitude or high intensity). The similarities in simulated flood characteristics suggests the possibility of developing design storms able of replicating the flood characteristics of Dominica from a real TC event. Since the high intensities scenarios where observed to give overall higher flood characteristics as compared to the high magnitude pixels, a conclusion can be made that rainfall intensity marks the most important factor in flood analysis.

Underlying choices influencing the flood characteristics results

When transposing the selected TC pixels, from the Caribbean Sea to Dominica, a choice was made to disregard any possible alteration in rainfall structure due to orographic influences (section 4.5). It is well noted that the decision made not to alter the rainfall structure may compromise the value of the method applied and the results obtained. However, since Dominica's design storms did not include orographic influence (Jetten, 2020; Personal correspondence), and the research intended to provide a fair comparison between the two datasets, the choice made not to alter the dataset is justifiable. One may argue on the option to factor in orographic effects on both datasets. This option was not possible as the factor of the orographic influence was not known. For complex rainfall structures such as the case with TCs, the orographic influence is difficult to isolate from a mixture of factors influencing rainfall (Houze et al., 2017; Kirshbaum & Smith, 2009; Nugent & Rios-Berrios, 2018). While the choice made to neglect orographic influences on rainfall structure may be justifiable, the failure to include orographic influence presents a limitation to the argument of a worst-case TC rainfall scenario.

Concerning the comparison made between the 100-year design storm and the TC scenarios. The two rainfall datasets were modelled on different temporal resolution. While it might have been logical to resample the 100-year design storm to a 30-minute resolution, this was not done. The decision made to simulate the two rainfall groups on different resolutions was so as to compare the TC rainfall characteristics with the actual flood characteristics being simulated in Dominica.

RQ2.3 What are the implications of the flood characteristics simulated from the selected design storm and the worst-case rainfall scenario of the TC?

Section 6.6 stated the flood implications from simulating the 100-year design storm against the worst-case TC rainfall scenario (INT-2). The implications addressed were, however, based solely on personal interpretation of the flood characteristic results linked to literature findings. The lack of expert judgement on evaluating the economic and social flood implications from simulating flood using either of the two approaches generally weakens the validity of the stated findings.

7.3 Reasearch relevance

With the occurrence of unprecedented TC rainfall events producing immense flooding (Emanuel, 2017; Ramos-Scharrón & Arima, 2019), the developed method will be highly useful in mitigating and preparing against future worst-case TC rainfall events. In a report published by the Intergovernmental Panel on Climate Change (IPCC, 2018), TCs are expected to decrease in frequency but increase in rainfall intensity and rain band extents. Although uncertain about the factual effects of climate change on TCs, the publication of the IPCC together with past studies on the effects of climate change on TCs (Bacmeister et al., 2018; Balaguru et al., 2018; Landsea et al., 2006; Mendelsohn, Emanuel, Chonabayashi, & Bakkensen, 2012; Ranson et al., 2014; Richard et al., 2006) prompt concerns on the sufficiency of historical events in mitigating against future TC flood hazards. Instead of relying on historical rainfall events to predict and mitigate against future events, the research presents a strategy to make use of currently observed TC rainfall characteristics. Through monitoring of TC rainfall characteristics, communities are not only able to observe trends in TC rainfall and mitigate against rainfall magnitudes occurring within neighbouring regions, but also increase TC understandings. One of the findings of this research for instance, showed the absence of a direct relationship between TC rainfall and the maximum wind speed of the cyclone. This finding bears vast significance especially when issuing out early warnings. Given the probability of worst-case rainfall scenarios developing from lower category cyclones, the research shows the need for officials to re-evaluate strategies of reporting early warnings by not only emphasizing warnings for higher TC categories. Additionally, the developed method allows for communities to assess the robustness of own design storms. By adopting the methodology presented in this research (Figure 7.1), communities can evaluate if the currently used design storms provide a sufficient replication of a TC flood hazard. In the absence of reliable rainfall measuring instruments, communities can make use of the suggested method in flood hazard forecasting.

CHAPTER 8 RECOMMENDATIONS

This research provided basis for future flood analysis using unprecedented TC rainfall events. Although the study presented a lot of interesting findings, several questions remain unanswered which present abundant room for further study. Since the TC rainfall extraction strategy was developed as a proof of concept, only a single TC was used. Future studies ought to consider expanding the number of TCs analysed to carter for the erratic nature of TCs. When selecting the TCs for analysis, researchers should aim to incorporate the influence of climatic conditions on rainfall structures by prioritizing the most recent TCs within the study basin.

The magnitude and intensity threshold values used to extract the extreme rainfall pixels of TC Maria were set with the intent to reduce the analysis as a proof of method. Since the developed strategy proved to be sufficient, future research need to find a valid approach to select threshold values for extracting extreme rainfall pixels. A strategy to extract extreme rainfall pixels can provide higher robustness of the method presented as it will allow for a complete analysis of the TC rainfall structures.

Regarding the flood analysis, the findings presented in this research highlighted the possibility of developing a design storm that could replicate TC flood characteristics. A further study can thus focus on evaluating different approaches used in creating design storms to find the best design storm structure that can provide feasible estimates of flood characteristics of real event storms. A step further would then be analyse the possibility of linking a return period to the extracted TC satellite rainfall estimates.

For the research's main objective which was to evaluate flood implications of simulating the design storm and the worst-case TC rainfall scenario, a recommendation is to make use of expert judgement. Future studies will have to consider carrying out interviews or seminars with experts on flood modelling for Dominica Island. The results obtained from expert judgements will have great influence on the decisions and conclusions made on the use of the design storms or presented strategy in this research.

In summary of the above stated, possible research questions to be addressed in future studies include but are not limited to the following:

Tropical cyclone precipitation analysis

- What strategy should be used to decide on the TCs to analyse?
- Is it possible to obtain return periods for spatial rainfall information?
- What approach should be taken to define the threshold for selecting extreme rainfall pixels?

Flood modelling

- How should design storms be created that can replicate the flood hazard from TC events?
- What strategy should be used to assign a return period to the TC scenarios?

LIST OF REFERENCES

Acevedo, S. (2016). *Gone with the Wind: Estimating Hurricane and Climate Change Costs in the Caribbean. IMF Working Papers* (Vol. 16). https://doi.org/10.5089/9781475544763.001

Adom, A. . (2018). Surviving Maria from Dominica: Memory, Displacement and Bittersweet Beginnings. *Transforming Anthropology*, *26*(2), 118–135. https://doi.org/10.1111/traa.12133

Agustín Breña-Naranjo, J., Pedrozo-Acuña, A., Pozos-Estrada, O., Jiménez-López, S. A., & López-López, M. R. (2015). The contribution of tropical cyclones to rainfall in Mexico. *Physics and Chemistry of the Earth*, *83–84*, 111–122. https://doi.org/10.1016/j.pce.2015.05.011

Aon Benfield Analytics. (2018). *Hurricane Maria Event Recap Report. Impact Forecasting.*

Bacmeister, J. T., Reed, K. A., Hannay, C., Lawrence, P., Bates, S., Truesdale, J. E., … Levy, M. (2018). Projected changes in tropical cyclone activity under future warming scenarios using a high-resolution climate model. *Climatic Change*, *146*(3–4), 547–560. https://doi.org/10.1007/s10584-016-1750-x

Balaguru, K., Foltz, G. R., & Leung, L. R. (2018). Increasing magnitude of hurricane rapid intensification in the central and eastern tropical Atlantic. *Geophysical Research Letters*, *45*(9), 4238–4247. https://doi.org/10.1029/2018GL077597

Balbastre-Soldevila, R., García-Bartual, R., & Andrés-Doménech, I. (2019). A comparison of design storms for urban drainage system applications. *Water (Switzerland)*, *11*(4), 1–15. https://doi.org/10.3390/w11040757

Barclay, J., Wilkinson, E., White, C. S., Shelton, C., Forster, J., Few, R., … Honychurch, L. (2019). Historical Trajectories of Disaster Risk in Dominica. *International Journal of Disaster Risk Science*, *10*(2), 149–165. https://doi.org/10.1007/s13753-019-0215-z

Beguería, S., & Vicente-Serrano, S. M. (2006). Mapping the hazard of extreme rainfall by peaks over threshold extreme value analysis and spatial regression techniques. *Journal of Applied Meteorology and Climatology*, *45*(1), 108–124. https://doi.org/10.1175/JAM2324.1

Begueria, S., Vicente-Serrano, S. M., Lopez-Moreno, J. I., & Garcia-Ruiz, J. M. (2009). Annual and seasonal mapping of peak intensity, magnitude and duration of extreme precipitation events across a climatic gradient, northeast Spain. *International Journal of Climatology*, *29*(12), 1759–1779. https://doi.org/10.1002/joc

Beguería, S., Vicente-Serrano, S. M., Lopez-Moreno, J. I., & Gracia-Ruiz, J. M. (2009). Annual and seasonal mapping of peak intensity, magnitude and duration of extreme precipitation events across a climatic gradient, northeast Spain. *International Journal of Climatology*, *29*(12), 1759–1779.

Blake, E. S., Landsea, C. W., Miami, N., & Gibney, E. J. (2011). NOAA Technical Memorandum NWS NHC-6 THE DEADLIEST, COSTLIEST, AND MOST INTENSE UNITED STATES TROPICAL CYCLONES FROM 1851 TO 2010, *2010*(August). Retrieved from https://www.nhc.noaa.gov/pdf/nws-nhc-6.pdf

Blake, E. S., & Zelinsky, D. A. (2018). *Hurricane Harvey. National Hurricane Center.* https://doi.org/AL092017

Bout, B., Jetten, V., De Roo, A., Wesseling, C., & Ritsema, C. (2018). OpenLISEM- Multi-Hazard Land Surface Process Model. Retrieved from https://blog.utwente.nl/lisem/

Chen, F. J., & Fu, Y. F. (2015). Contribution of tropical cyclone rainfall at categories to total precipitation over the Western North Pacific from 1998 to 2007. *Science China Earth Sciences*, *58*(11), 2015–2025. https://doi.org/10.1007/s11430-015-5103-9

Chen, S. S., Knaff, J. A., & Marks, F. D. (2006). Effects of vertical wind shear and storm motion on tropical cyclone rainfall asymmetries deduced from TRMM. *Monthly Weather Review*, *134*(11), 3190–3208. https://doi.org/10.1175/MWR3245.1

Collymore, J. (2011). Disaster management in the Caribbean: Perspectives on institutional capacity reform and development. *Environmental Hazards*, *10*(1), 6–22. https://doi.org/10.3763/ehaz.2011.0002

Czajkowski, J., Villarini, G., Michel-Kerjan, E., & Smith, J. A. (2013). Determining tropical cyclone inland flooding loss on a large scale through a new flood peak ratio-based methodology. *Environmental Research Letters*, *8*(4). https://doi.org/10.1088/1748-9326/8/4/044056

de Barros, C. A. P., Minella, J. P. G., Dalbianco, L., & Ramon, R. (2014). Description of hydrological and erosion processes determined by applying the LISEM model in a rural catchment in southern Brazil. *Journal of Soils and Sediments*, *14*(7), 1298–1310. https://doi.org/10.1007/s11368-014-0903-7

de Paola, F., Giugni, M., Topa, M. E., & Bucchignani, E. (2014). Intensity-Duration-Frequency (IDF)

rainfall curves, for data series and climate projection in African cities. *SpringerPlus*, *3*(1), 1–18. https://doi.org/10.1186/2193-1801-3-133
Doswell III, C. A. (2015). Flooding. In *Hydrology, floods and droughts* (Second Edi, pp. 201–208). Oklahoma: Encyclopedia of Atmospheric Sceience, Elsevier Ltd. https://doi.org/https://doi.org/10.1016/B978-0-12-382225-3.00151-1
Emanuel, K. (2017). Assessing the present and future probability of Hurricane Harvey's rainfall. *Proceedings of the National Academy of Sciences of the United States of America*, *114*(48), 12681–12684. https://doi.org/10.1073/pnas.1716222114
Fattorelli, S., Dalla Fontana, G., & Da Ras, D. (1999). Flood Hazard Assessment and Mitigation. In R. Casale & C. Margottini (Eds.), *Floods and Landslides: Integrated Risk Assessment* (1st ed., p. 373). Springer Science & Business Media. https://doi.org/10.1007/978-3-642-58609-5
Goldenberg, S. B., Landsea, C. W., Mestas-Nuñez, A. M., & Gray, W. M. (2001). The recent increase in Atlantic hurricane activity: Causes and implications. *Science*, *293*(5529), 474–479. https://doi.org/10.1126/science.1060040
Gomes, N. M., Mello, C. R. de, Silva, A. M. da, & Beskow, S. (2009). Applicability of the LISEM (Limburg Soil Erosion Model) model for hydrological simulation in a tropical watershed. *Revista Brasileira de Ciencia Do Solo*, *32*(6), 2483–2492. https://doi.org/10.1590/S0100-06832008000600025
Government of the Commonwealth of Dominica, & Damage. (2015). *Rapid Damage and Impact Assessment Tropical Storm Erika – August 27 , 2015 A Report by the Government of the Commonwealth of Dominica*. *GFDRR*.
Grum, B., Woldearegay, K., Hessel, R., Baartman, J. E. M., Abdulkadir, M., Yazew, E., … Geissen, V. (2017). Assessing the effect of water harvesting techniques on event-based hydrological responses and sediment yield at a catchment scale in northern Ethiopia using the Limburg Soil Erosion Model (LISEM). *Catena*, *159*(July), 20–34. https://doi.org/10.1016/j.catena.2017.07.018
Houze, R. A., McMurdie, L. A., Petersen, W. A., Schwall Er, M. R., Baccus, W., Lundquist, J. D., … Barnes, H. C. (2017). The olympic mountains experiment (Olympex). *Bulletin of the American Meteorological Society*, *98*(10), 2167–2188. https://doi.org/10.1175/BAMS-D-16-0182.1
Huffman, G. J., Stocker, E. F., Bolvin, D. T., Nelkin, E. J., & Jackson, T. (2019). GPM IMERG Early Precipitation L3 Half Hourly 0.1 degree * 0.1 degree V06. https://doi.org/10.5067/GPM/IMERG/3B-HH-E/06
IPCC. (2018). *Global warming of 1.5 degree celcius. An IPCC Special Report on the impacts of global warmining of 1.5 degrees celcius above pre-industrial levels and related global greenhouse gas emission pathways, in the contect of strengthening the global response to* . https://doi.org/10.1038/291285a0
Jamrussri, S., & Toda, Y. (2018). Available flood evacuation time for high-risk areas in the middle reach of Chao Phraya River Basin. *Water*, *10*(12), 1–23. https://doi.org/10.3390/w10121871
Jayawardena, A. W. (2015). Hydro-meteorological Disasters: Causes, Effects and Mitigation Measures with Special Reference to Early Warning with Data Driven Approaches of Forecasting. *Procedia IUTAM*, *17*(September 2013), 3–12. https://doi.org/10.1016/j.piutam.2015.06.003
Jetten, V. (2016). *CHARIM National Flood Hazard Map Dominica*. *ACP-EU Natural Disaster Risk Reduction Program, World Bank*. ITC Faculty, Enschede.
Jiang, H., Halverson, J. B., Simpson, J., & Zipser, E. J. (2008). Hurricane "rainfall potential" derived from satellite observations aids overland rainfall prediction. *Journal of Applied Meteorology and Climatology*, *47*(4), 944–959. https://doi.org/10.1175/2007JAMC1619.1
Jonkman, S. N, Vrijling, K. S., & Vrouwenvelder, A. C. W. M. (2008). Methods for the estimation of loss of life due to floods : a literature review and a proposal for a new method. *Natural Hazards*, *46*, 353–389. https://doi.org/10.1007/s11069-008-9227-5
Jonkman, Sebastiaan N., Maaskant, B., Boyd, E., & Levitan, M. L. (2009). Loss of life caused by the flooding of New Orleans after hurricane Katrina: Analysis of the relationship between flood characteristics and mortality. *Risk Analysis*, *29*(5), 676–698. https://doi.org/10.1111/j.1539-6924.2008.01190.x
Khan, S., & Maggioni, V. (2019). Assessment of level-3 Gridded Global Precipitation Mission (GPM) products over oceans. *Remote Sensing*, *11*(3), 17. https://doi.org/10.3390/rs11030255
Kim, K., Pant, P., & Yamashita, E. (2014). Evacuation planning for plausible worst case inundation scenarios in Honolulu, Hawaii. *Emergency Management*, *12*(4), 1–17. https://doi.org/10.5055/jem.2014.0000
Kirshbaum, D. J., & Smith, R. B. (2009). Orographic precipitation in the tropics: Large-Eddy simulations and theory. *Journal of the Atmospheric Sciences*, *66*(9), 2559–2578.

https://doi.org/10.1175/2009JAS2990.1
Klotzbach, P. J., Schreck, C. J., Collins, J. M., Bell, M. M., Blake, E. S., & Roache, D. (2018). The extremely active 2017 North Atlantic hurricane season. *Monthly Weather Review*, *146*(10), 3425–3443. https://doi.org/10.1175/MWR-D-18-0078.1
Knapp, K. R., Kruk, M. C., Levinson, D. H., Diamond, H. J., & Neumann, C. J. (2010). The international best track archive for climate stewardship (IBTrACS). *Bulletin of the American Meteorological Society*, *91*(3), 363–376. https://doi.org/10.1175/2009BAMS2755.1
Knight, D. B., & Davis, R. E. (2009). Contribution of tropical cyclones to extreme rainfall events in the southeastern United States. *Journal of Geophysical Research Atmospheres*, *114*(23), 1–17. https://doi.org/10.1029/2009JD012511
Landsea, C. W., Harper, B. A., Hoarau, K., & Knaff, J. A. (2006). Can we detect trends in extreme tropical cyclones? *Science*, *313*(5786), 452–454. https://doi.org/10.1126/science.1128448
Lonfat, M., Marks Jr, F. D., & Chen, S. S. (2004). Precipitation Distribution in Tropical Cyclones Using the Tropical Rainfall Measuring Mission (TRMM) Microwave Imager: A Global Perspective. *Monthly Weather Review*, *132*, 1645–1660. https://doi.org/https://doi.org/10.1175/1520-0493(2004)132<1645:PDITCU>2.0.CO;2
Lumbroso, D. M., Boyce, S., Bast, H., & Walmsley, N. (2011). The challenges of developing rainfall intensity-duration-frequency curves and national flood hazard maps for the Caribbean. *Journal of Flood Risk Management*, *4*(1), 42–52. https://doi.org/10.1111/j.1753-318X.2010.01088.x
Mendelsohn, R., Emanuel, K., Chonabayashi, S., & Bakkensen, L. (2012). The impact of climate change on global tropical cyclone damage. *Nature Climate Change*, *2*(3), 205–209. https://doi.org/10.1038/nclimate1357
Meteorological Department Curacao. (2015). *Hurricanes and Tropical Storms in the Dutch Caribbean*.
Meteorological Department Curacao. (2017). *GUIDE ON THE TROPICAL CYCLONE EARLY WARNING SYSTEM*.
National Hurricane Center. (2018). Costliest U.S. tropical cyclones tables updated. *NOAA Technical Memorandum NWS NHC-6*. NOAA. Retrieved from https://www.nhc.noaa.gov/news/UpdatedCostliest.pdf
Nugent, A. D., & Rios-Berrios, R. (2018). Factors leading to extreme precipitation on dominica from Tropical Storm Erika (2015). *Monthly Weather Review*, *146*(2), 525–541. https://doi.org/10.1175/MWR-D-17-0242.1
Ogden, F. L. (2016). Evidence of equilibrium peak runoff rates in steep tropical terrain on the island of Dominica during Tropical Storm Erika, August 27, 2015. *Journal of Hydrology*, *542*, 35–46. https://doi.org/10.1016/j.jhydrol.2016.08.041
Opper, S., Cinque, P., & Daviesc, B. (2010). Timeline modelling of flood evacuation operations. *Procedia Engineering*, *3*, 175–187. https://doi.org/10.1016/j.proeng.2010.07.017
Pasch, R. J., Penny, A. B., & Berg, R. (2019). *Hurricane Maria (AL152017). National Hurricane Center Tropical Cyclone Report*.
Paul-Rolle, A. (2014). *Disaster Risk Reduction Country Profile, Dominca 2014*.
Pielke, R. A. (2005). Are there trends in hurricane destruction? *Nature*, *438*(7071), E11–E11. https://doi.org/10.1038/nature04426
Prevatt, D. O., Dupigny-Giroux, L. A., & Masters, F. J. (2010). Engineering perspectives on reducing hurricane damage to housing in CARICOM Caribbean islands. *Natural Hazards Review*, *11*(4), 140–150. https://doi.org/10.1061/(ASCE)NH.1527-6996.0000017
Qi, Y., Martinaitis, S., Zhang, J., & Cocks, S. (2016). A real-time automated quality control of hourly rain gauge data based on multiple sensors in MRMS system. *Journal of Hydrometeorology*, *17*(6), 1675–1691. https://doi.org/10.1175/JHM-D-15-0188.1
Ramos-Scharrón, C. E., & Arima, E. (2019). Hurricane María's Precipitation Signature in Puerto Rico: A Conceivable Presage of Rains to Come. *Scientific Reports*, *9*(1), 1–7. https://doi.org/10.1038/s41598-019-52198-2
Ranson, M., Kousky, C., Ruth, M., Jantarasami, L., Crimmins, A., & Tarquinio, L. (2014). Tropical and extratropical cyclone damages under climate change. *Climatic Change*, *127*(2), 227–241. https://doi.org/10.1007/s10584-014-1255-4
Rappaport, E. N. (2014). Fatalities in the United States from Atlantic Tropical Cyclones: New data and interpretation. *Bulletin of the American Meteorological Society*, *95*(3), 341–346. https://doi.org/10.1175/BAMS-D-12-00074.1
Rappaport, E. N., & Blanchard, B. W. (2016). Fatalities in the United States indirectly associated with

Atlantic tropical cyclones. *Bulletin of the American Meteorological Society*, *97*(7), 1139–1148. https://doi.org/10.1175/BAMS-D-15-00042.1
Richard, A. A., Robert W. COrell, Greg Holland, James W. Hurrell, Michael C. Mac Cracken, & Kevin E. Trenberth. (2006). Hurrricanes and Global Warming - Potential Linkages and Consequences. *Bulletin of the American Meteorological Society*, *87*(5), 623–632. https://doi.org/10.1175/BAMS-87-5-617
Roy, C., Sarkar, S. K., Åberg, J., & Kovordanyi, R. (2015). The current cyclone early warning system in Bangladesh: Providers' and receivers' views. *International Journal of Disaster Risk Reduction*, *12*(June 2018), 285–299. https://doi.org/10.1016/j.ijdrr.2015.02.004
Schnitter, R., Verret, M., Berry, P., Fook, T. C. T., Hales, S., Lal, A., & Edwards, S. (2019). An assessment of climate change and health vulnerability and adaptation in dominica. *International Journal of Environmental Research and Public Health*, *16*(1). https://doi.org/10.3390/ijerph16010070
Smith, R. B., Minder, J. R., Nugent, A. D., Storelvmo, T., Kirshbaum, D. J., Warren, R., … French, J. (2012). Orographic Precipitation in the Tropics: The Dominica Experiment. *Bulletin of the American Meteorological Society*, *93*(10), 1567–1579. https://doi.org/10.1175/BAMS-D-11-00194.1
Starkloff, T., Stolte, J., Hessel, R., Ritsema, C., & Jetten, V. (2018). Integrated, spatial distributed modelling of surface runoff and soil erosion during winter and spring. *Catena*, *166*(October 2017), 147–157. https://doi.org/10.1016/j.catena.2018.04.001
Stewart, S. R. (2017). *Hurricane Matthew. National Hurricane Center*. https://doi.org/AL142016
Tan, J., Petersen, W. A., & Tokay, A. (2016). A novel approach to identify sources of errors in IMERG for GPM ground validation. *Journal of Hydrometeorology*, *17*(9), 2477–2491. https://doi.org/10.1175/JHM-D-16-0079.1
Tapsell, S., Mccarthy, S., Faulkner, H., Alexander, M., Kuhlicke, C., Brown, S., … Bianchizza, C. (2010). *Social Vulnerability and Natural Hazards. CapHaz-Net WP4 Report, Flood Hazard Research Centre (FHRC)*. London. Retrieved from http://citeseerx.ist.psu.edu/viewdoc/download?doi=10.1.1.471.849&rep=rep1&type=pdf%0Ahttp://caphaz-net.org/outcomes-results/CapHaz-Net_WP4_Social-Vulnerability2.pdf
Teitelbaum, L., Ginsburg, M. L., & Hopkins, R. W. (2015). Sendai Framework for Disaster Risk Reduction 2015 - 2030. *United Nations*, *144*(2), 169–173.
Tennant, W. J., & Hewitson, B. C. (2002). Intra-seasonal rainfall characteristics and their importance to the seasonal prediction problem. *International Journal of Climatology*, *22*(9), 1033–1048. https://doi.org/10.1002/joc.778
The World Bank. (2012). *Disaster Risk Management in Latin America and the Caribbean Region: GFDRR Country Notes Dominica*. https://doi.org/10.1596/27336
Tokay, A., & Öztürk, K. (2012). An experimental study of the small-scale variability of rainfall. *Journal of Hydrometeorology*, *13*(1), 351–365. https://doi.org/10.1175/JHM-D-11-014.1
Wang, J., & Wolff, D. B. (2012). Evaluation of TRMM rain estimates using ground measurements over central Florida. *Journal of Applied Meteorology and Climatology*, *51*(5), 926–940. https://doi.org/10.1175/JAMC-D-11-080.1
Ybañez, R. (2013). Understanding Rainfall Return Periods. *Project NOAH Open-File Reports*, *1*(2), 3–4. https://doi.org/ISSN 2362 7409
Zhou, Y., & Matyas, C. J. (2018). Spatial Characteristics of Rain Fields Associated with Tropical Cyclones Landfalling over the Western Gulf of Mexico and Caribbean Sea. *Journal of Applied Meteorology and Climatology*, *57*, 1711–1727. https://doi.org/10.1175/JAMC-D-18-0034.1

APPENDIX

Appendix 1: Selection of the GPM IMERG run

The results of the recorded maximum rainfall estimated for the GPM IMERG Early, Late and Final runs for 2016 TC Matthew and 2017 TC Maria are shown in Figure 8.1. For TC Matthew, NHC ground observations show, in comparison to the GPM IMERG runs, much larger rainfall totals for the islands of Haiti, Dominica Republic and Cuba, whilst recording the least rainfall for Martinique. For TC Maria, the NHC records the highest rainfall estimates for Dominica and Puerto Rico and the least totals, of the comparison, for Guadeloupe and Dominica Republic. As for the GPM IMERG runs, maximum recorded rainfalls fluctuate with each run. For TC Matthew, the GPM IMERG early run shows rainfall estimate values closer to the NHC data for Martinique and Haiti islands, whilst the final run showed values closer to the NHC in Dominica republic and the late run being closer to NHC rainfall estimates in Cuba. For Tropical cyclone Maria, the GPM IMERG final run gave maximum values closer to the NHC for Dominica, Guadeloupe, and Dominica republic. However, in Puerto Rico, IMERG final run showed the largest difference with the NHC in comparison to the early and late run.

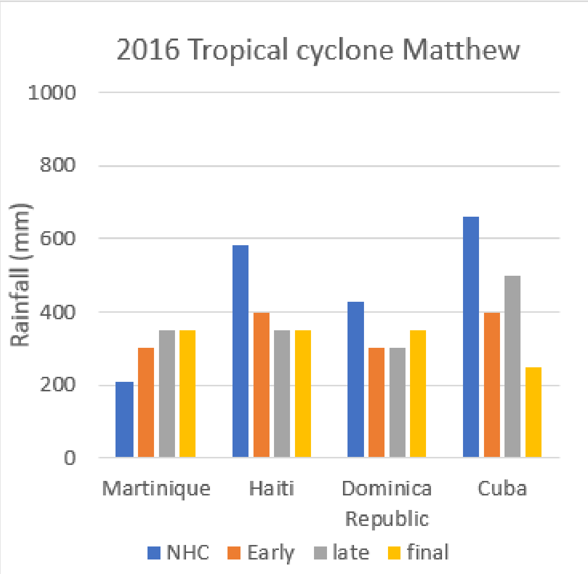

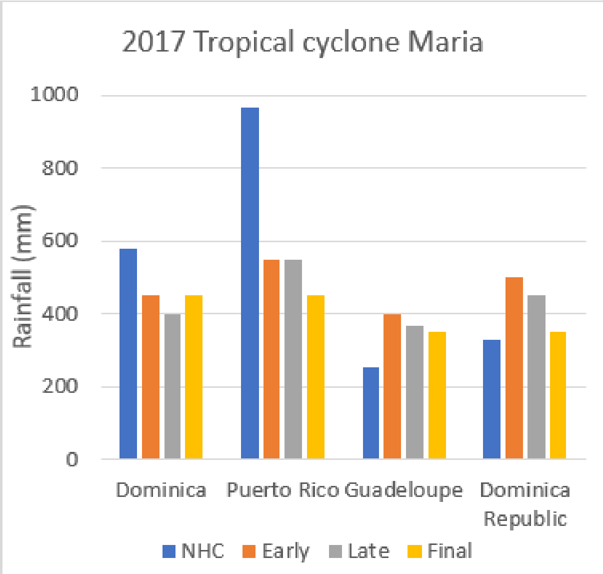

Figure 8.1 Maximum rainfall estimates obtained from the passing of 2016 TC Matthew (left) and 2017 TC Maria (right) as recorded by the National Hurricane Centre (NHC) synoptic reports and the GPM IMERG Early, late and, Final runs for selected Islands within the Caribbean sea.

Due to the fluctuations in the closeness of the IMERG runs to the NHC observations, no selection was made based on the comparison results in Figure 8.1. However, an enquiry was made to NASA personnel, George Huffman (18.10.2019) as to the differences of the rainfall magnitudes from the IMERG runs, and the NHC reports. George Huffman explained that the GPM IMERG Final dataset has a calibration centred on monthly data hence possibly giving over or underestimates in some areas. George Huffman also highlighted that although rain gauge calibration is supposed to be an adequate bias correcting factor, a lot of rain gauge stations in Puerto Rico, for instance, were overwhelmed and destroyed during TC Maria thus making it difficult to obtain proper calibration values. In general, the accuracy of the ground observations, especially in extreme events such as the case with tropical cyclones, are highly questionable (Qi et al., 2016) making accurate precipitation values almost always impossible to find in both gauge data and satellite data. For these reasons, the GPM IMERG Final run, precipitation estimates were accepted as the best available dataset for this research, and despite the discrepancy between the IMERG Final dataset and the ground data, no bias correction was applied.

Appendix 2: R script for precipitation computations

```
# load libraries
library('spatial')
library('stats')
library('graphics')
library('gdata')
library('raster')
library('rgdal')
library('sp')
library('ncdf4')
library('dplyr')
library('ggplot2')
library('stringr')
#Including only tropical cyclone related rainfall values
# set working directory
project_dir <- 'add directory path'

#import all files in a single folder as a list
rastlist <- list.files(path = paste(project_dir, 'rast_Folder', sep='/'),
pattern='.tif$', all.files=TRUE, full.names=FALSE)

# mask each raster using a corresponding shapefile
for (raster_file in rastlist) {
 vector_file <- str_replace(str_replace(raster_file, '.tif', '.shp'), 'x_',
'')
 vector_file <- paste(project_dir, '30minute', 'complete_shp', vector_file,
sep='/')
 output_file <- paste(project_dir, 'cropped', raster_file, sep='/')
 raster_file <- paste(project_dir, 'rast_Folder', raster_file, sep='/')

 print(raster_file)
 print(vector_file)

 rast <- raster(raster_file)
 vect <- readOGR(vector_file)

 print(vector_file)

 cropped <- mask(rast, vect)
 plot(cropped)

 writeRaster(cropped, filename = output_file, overwrite = TRUE)
}
```

- The cropped files are added to base map to equalise spatial extent in ArcMap.

```
#Putting the raster images into correct order stacked
setwd("C:/Users/helen/Documents/1Thesis/images")
images <- list.files(path = ".", pattern = "tif$", full.names = FALSE)
split <- as.numeric(sapply(images, function(x) x <- sub(".tif", "", x[1])))
myImages.correct.order <- images[order(split)]
My_Rast <- stack(myImages.correct.order)


 #Computing for TC Maria's magnitude
Total <- sum(My_Rast)
Magnitude <- (Total/2)
plot(Magnitude)
which(Magnitude[,] > 750, arr.ind = T)
```

```
# Maximum intensity values
maxValue(rast)
which((maxValue(rast)) >100)
```

Appendix 3: LISEM run options

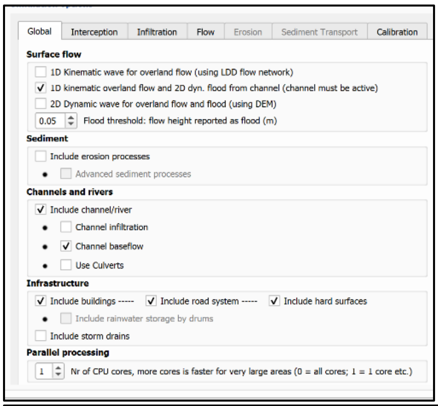

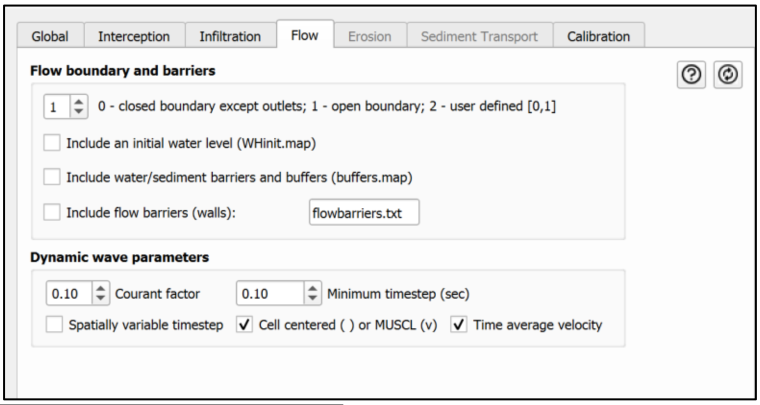

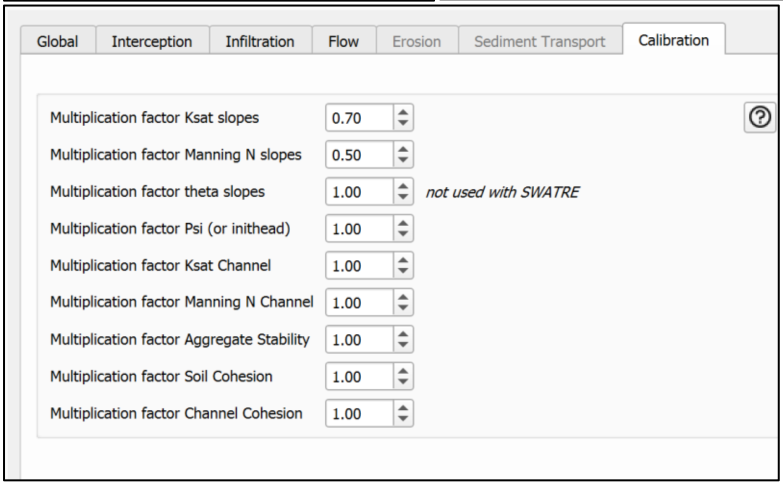

Appendix 4: pc raster computations for flood characteristics

```
pcrcalc wsvol.map=areatotal(if(whmax.map gt
0.05,whmax.map*cellarea(),0),ws.map)
```

Equation 1: Calculation of the flood volume in pc raster.

```
pcrcalc wsarea.map=areatotal(if(whmax.map gt
0.05,cellarea(),0),ws.map)
```

Equation 2: Calculation of flood extent in pc raster.

Appendix 5: Infiltration maps for the five rainfall scenarios

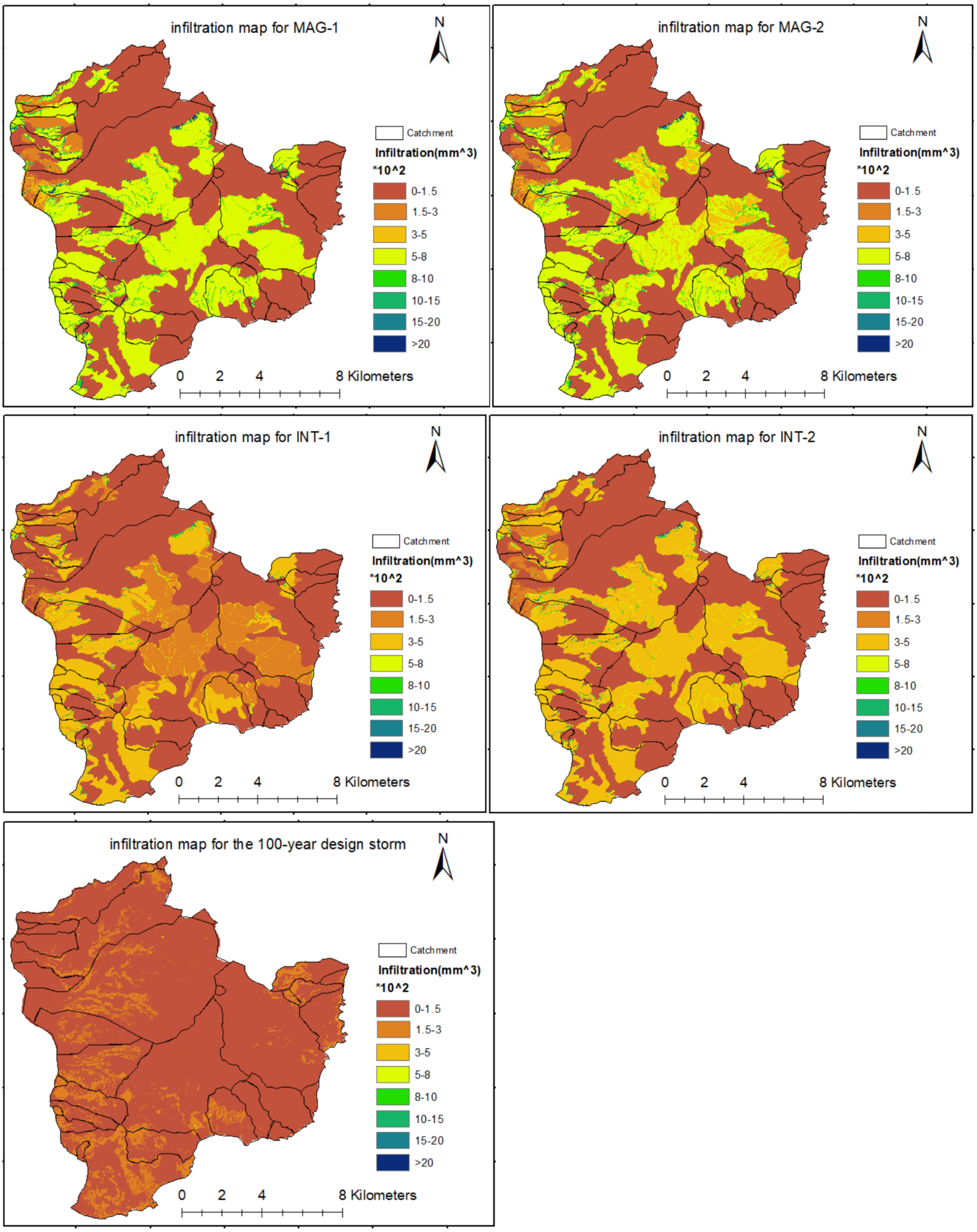

The high intensity scenarios show a lower infiltration rate compared to the high magnitude scenarios with lower intensity. The design storm scenario shows the least infiltration of the 5 scenarios.